



## Inhibition of NLRP3-mediated crosstalk between hepatocytes and liver macrophages by geniposidic acid alleviates cholestatic liver inflammatory injury

Meng Song<sup>a,b</sup>, Zijun Chen<sup>a</sup>, Ruian Qiu<sup>a</sup>, Tingwei Zhi<sup>a</sup>, Wenmin Xie<sup>a</sup>, Yingya Zhou<sup>a</sup>, Nachuan Luo<sup>c</sup>, Fuqian Chen<sup>a</sup>, Fang Liu<sup>a</sup>, Chuangpeng Shen<sup>d</sup>, Sheng Lin<sup>e,\*\*\*\*</sup>, Fengxue Zhang<sup>b,\*\*\*</sup>, Yong Gao<sup>f,g,\*\*</sup>, Changhui Liu<sup>a,\*</sup>

<sup>a</sup> School of Pharmaceutical Sciences, Guangzhou University of Chinese Medicine, Guangzhou, 510405, China

<sup>b</sup> School of Basic Medical Sciences, Guangzhou University of Chinese Medicine, Guangzhou, 510405, China

<sup>c</sup> Guangdong Provincial Key Laboratory of Virology, Institute of Medical Microbiology, Jinan University, Guangzhou, 510632, China

<sup>d</sup> The First Affiliated Hospital of Guangzhou University of Chinese Medicine, Guangzhou University of Chinese Medicine, Guangzhou, 510405, China

<sup>e</sup> Key Laboratory of Chinese Internal Medicine of Ministry of Education and Beijing, Dongzhimen Hospital, Beijing University of Chinese Medicine, Beijing, 100700, China

<sup>f</sup> Science and Technology Innovation Center, Guangzhou University of Chinese Medicine, Guangzhou, 510405, China

<sup>g</sup> Division of Hypothalamic Research, Department of Internal Medicine, The University of Texas Southwestern Medical Center at Dallas, Dallas, TX, USA

### ABSTRACT

The excessive accumulation of bile acids (BA) in hepatocytes can trigger inflammatory response and recruit macrophages, thereby accelerating cholestatic liver injury. The crosstalk between hepatocytes and macrophages has been recently implicated in the pathogenesis of cholestasis; however, the underlying mechanisms remain unclear. Here, we demonstrated that BA initiate NLRP3 inflammasome activation in hepatocytes to release proinflammatory cytokines and promote the communication between hepatocytes and macrophages, thus enhancing liver inflammation in an NLRP3-dependent manner. NLRP3-inhibition by geniposidic acid (GPA), a novel NLRP3-specific covalent inhibitor that directly interacts with NLRP3, in hepatocytes and macrophages abated BA-induced inflammation. Moreover, NLRP3-deletion or its inhibition mitigated ANIT-induced cholestatic inflammation, whereas disrupting the crosstalk between hepatic macrophages and hepatocytes attenuated the hepatoprotective effect of GPA against ANIT-induced cholestatic inflammation. Therefore, blocking this crosstalk by suppressing NLRP3 inflammasome activation may represent a novel therapeutic strategy for cholestasis.

### 1. Introduction

Cholestasis refers to the impairment of bile formation or bile flow due to reduced secretion by hepatocytes or obstruction of the intra- or extrahepatic bile ducts, thus leading to the excessive accumulation of BA and other toxic metabolites in the liver and systemic circulation [1], which is a common secondary pathological feature of chronic liver disease.

$\alpha$ -naphthalene isothiocyanate (ANIT)-induced acute intracholestasis

is the standard experimental model for studying sclerosing cholangitis resembling PSC [2]. ANIT causes complete biliary impairment and obstruction and the accumulation of toxic BAs in the liver and serum of patients. However, the etiology and pathogenic mechanisms of cholestasis remain largely unclear, which contributes to the lack of effective therapies aside from liver transplantation. To date, ursodeoxycholic acid (UDCA) is the only available first-line drug against cholestasis, and its efficacy is limited in some circumstances [3]. Therefore, novel drugs need to be developed urgently.

**Abbreviations:** alanine aminotransferase, ALT;  $\alpha$ -naphthalene isothiocyanate, ANIT; apoptosis-associated speck-like protein, ASC; aspartate transaminase, AST;  $\beta$ -mercaptoethanol,  $\beta$ -Me; bile acids, BA; bile duct ligation, BDL; biotinylated GPA, bio-GPA; bone-marrow-derived macrophage, BMDM; geniposidic acid, GPA; Kupffer cells, KCs; NOD-like receptor protein 3, NLRP3; primary mouse hepatocytes, PMHs; primary sclerosing cholangitis, PSC; taurocholic acid, TCA; total bile acid, TBA; total bilirubin, TBIL.

\* Corresponding author. School of Pharmaceutical Sciences, Guangzhou University of Chinese Medicine, No 12, Jichang Road, Guangzhou, 510405, China.

\*\* Corresponding author. Science and Technology Innovation Center, Guangzhou University of Chinese Medicine, Guangzhou, 510405, China.

\*\*\* Corresponding author.

\*\*\*\* Corresponding author.

E-mail addresses: [lsznn@126.com](mailto:lsznn@126.com) (S. Lin), [zhangfengxue@gzucm.edu.cn](mailto:zhangfengxue@gzucm.edu.cn) (F. Zhang), [gaoyong@gzucm.edu.cn](mailto:gaoyong@gzucm.edu.cn) (Y. Gao), [liuchanghui@gzucm.edu.cn](mailto:liuchanghui@gzucm.edu.cn) (C. Liu).

<https://doi.org/10.1016/j.redox.2022.102404>

Received 2 June 2022; Received in revised form 1 July 2022; Accepted 10 July 2022

Available online 14 July 2022

2213-2317/© 2022 The Authors. Published by Elsevier B.V. This is an open access article under the CC BY-NC-ND license (<http://creativecommons.org/licenses/by-nc-nd/4.0/>).

Recently, inflammation has been revealed to play an essential role in the pathogenesis of cholestatic liver injury. High concentrations of BAs in the liver can trigger the generation of proinflammatory cytokines in hepatocytes to initiate an inflammatory response [4]. NOD-like receptor protein 3 (NLRP3), the most well characterized and investigated inflammasome, is a multiprotein cytoplasmic complex containing apoptosis-associated speck-like protein (ASC) and the effector molecule pro-caspase-1 [5]. NLRP3 activation is induced by various stimuli, including pathogens and sterile insults, and mainly occurs via the generation of mitochondria-derived ROS or cathepsin B activation and deubiquitination [6]. Upon stimulation, NLRP3 binds to ASC and assembles the inflammasome complex, leading to caspase-1 activation, which subsequently proteolytically activates the IL-1 $\beta$  and IL-18 [7]. Particularly, NLRP3 is activated in the liver of patients with cholestasis or cholestatic mice [8,9], thereby suggesting its crucial role in cholestatic liver injury [10,11]. Moreover, NLRP3 deficiency or its inhibition by MCC950, a specific NLRP3 inhibitor, significantly mitigated liver injury and slowed the development of hepatic fibrosis in cholestasis mice induced by bile duct ligation (BDL) [8,11], thus indicating that the inhibition of NLRP3 inflammasome activation may represent a potential therapeutic route for cholestatic liver injury.

However, studies on the role of BAs in the regulation of NLRP3 inflammasome are controversial. Most report displayed that BAs could activate NLRP3 inflammasome [8,12], whereas another suggested that BAs could suppress NLRP3 inflammasome activation [12]. Such contradictory results suggested that the activation of NLRP3 by BA might be probably associated with the specific type of BAs used in a cell model, and highlighted the intricate function of BA-mediated activation of NLRP3 inflammasome in cholestasis. Notably, the BAs used for stimulating macrophages or hepatocytes were not the principal endogenous BAs in mice, or the used concentrations of BAs were not pathophysiologically relevant in these studies. However, whether BA-triggered inflammatory response is associated with the activation of the NLRP3 inflammasome in hepatocytes and liver macrophages remains unclear. In addition, the role of the NLRP3 inflammasome in ANIT-induced intrahepatic cholestatic inflammatory liver injury has not yet been investigated.

Here, we demonstrated, for the first time, that the major endogenous pathophysiologically relevant BA taurocholic acid (TCA) could activate NLRP3 inflammasome activation both in the primary mice hepatocytes (PMH) and bone marrow-derived monocytes (BMDM)-differentiated macrophages, thus triggering inflammation in hepatocytes and macrophages via an NLRP3-dependent mechanism. Furthermore, ANIT-induced intrahepatic cholestasis was attenuated by suppression of NLRP3 inflammasome activation via blockage of the crosstalk between hepatocytes and hepatic macrophages or deletion of hepatic macrophages. In contrast, liver-specific NLRP3 overexpression-mediated reinforcement of the mutual communication between hepatocytes and hepatic macrophages could contribute to intensified ANIT-induced cholestatic inflammatory injury. Finally, we identified a naturally occurring iridoid glycoside geniposidic acid (GPA) from *Gardeniae jasminoides* Ellis (Rubiaceae) and *Oldenlandia diffusa* Roxb, as a specific inhibitor of the NLRP3 inflammasome by covalently binding to NLRP3, thereby reducing ANIT-induced cholestatic liver inflammatory injury by disconnecting the crosstalk between hepatocytes and macrophages. Comprehensively, our results underline the importance of TCA-mediated NLRP3 inflammasome activation in intrahepatic cholestatic inflammatory injury, and the development of a novel NLRP3 inflammasome inhibitor may contribute to alleviating intrahepatic cholestasis.

## 2. Results

### 2.1. GPA directly binds to NLRP3 and represses its activity

We first investigated whether GPA can bind to NLRP3 using molecular docking analysis and confirmed the interaction of GPA with the

active site of NLRP3 (Fig. S1). Hydrogen bond formation with ALA85 and ASP88 and hydrophobic interactions between PHE73, MET56, LEU8, and ALA69 of the 2naq protein residues (PDB\_ID) with a high total score of 8.3906 and CSCORE of 4 were observed. Furthermore, GPA pretreatment significantly inhibited the NLRP3-luc promoter luciferase activity (Fig. 1A). Consistently, GPA reduced the mRNA levels of *NLRP3*, *NF $\kappa$ B1* and *IL-1 $\beta$*  in THP-1 and BMDM cells (Fig. 1B). Similar to the mRNA levels, the levels of protein, including NLRP3, ASC, and CASP-1, were significantly decreased by GPA pretreatment with the appropriate concentration (Fig. 1C).

As the chemical structure of GPA naturally harbors an  $\alpha,\beta$ -unsaturated carbonyl unit, which could easily carry out the Michael addition reaction by binding to the thiol group of cysteine in the NACHT domain of NLRP3 [13]. We found that noncovalent interactions can serve as an initial site-recognition step during the binding between GPA and NLRP3 (Fig. S1), thereby increasing the likelihood of a covalent binding. Interestingly, in the cell lysates of LPS-primed THP-1 monocytes, NLRP3, but not ASC, was pulled down by synthesized biotinylated GPA (bio-GPA) (Fig. 1D). Moreover, the pull-down of NLRP3 by bio-GPA could be competed with free GPA (Fig. 1E).

To further offer the evidence for GPA binding directly to NLRP3, purified NLRP3 proteins were incubated with bio-GPA. We observed that NLRP3 was pulled down by bio-GPA (Fig. 1F), verifying the direct interaction between GPA and NLRP3. To further address the importance of the  $\alpha,\beta$ -unsaturated carbonyl group in the inhibitory effect of GPA on NLRP3 inflammasome activation, bio-GPA was pre-incubated with  $\beta$ -mercaptoethanol ( $\beta$ -Me) to saturate the disulfide bonds. Notably,  $\beta$ -Me pretreatment completely blocked the pull-down of NLRP3 by Bio-GPA (Fig. 1). Overall, these results demonstrate that GPA can covalently target NLRP3 via a Michael acceptor mechanism by reacting with the thiol group of cysteine in the NACHT domain of NLRP3, thereby inhibiting its activity.

### 2.2. GPA reduces NLRP3 expression by suppressing NF- $\kappa$ B signaling in LPS-primed macrophages

Given that GPA physiologically inhibits NLRP3 expression (Fig. 1B and C), promoting us to investigate how GPA suppresses NLRP3 expression. We pretreated THP-1-derived macrophages and BMDM with GPA, followed by stimulation with LPS. GPA pretreatment substantially attenuated LPS-induced NLRP3 expression at both the mRNA and protein levels (Fig. 2A and B and Fig. S2). Furthermore, the release of pro-inflammatory cytokines, including IL-1 $\beta$ , IL-6, and TNF- $\alpha$ , was markedly blunted by GPA pretreatment prior to LPS stimulation (Fig. 2C). Similar results were found in BMDM as indicated by decreased genes expression and pro-inflammatory cytokines generation (Fig. 2D and E).

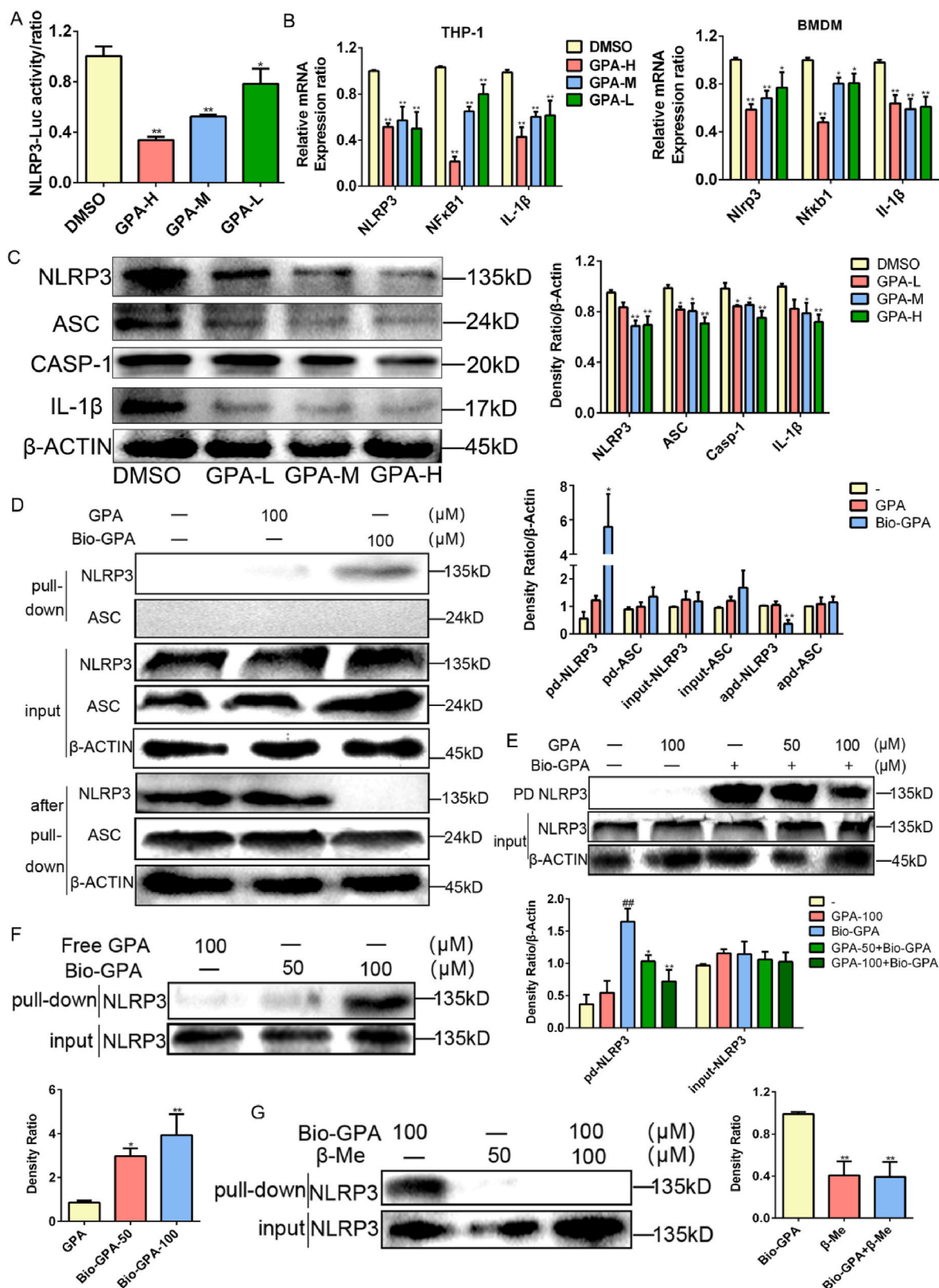
To further investigate the role of NLRP3 in the GPA-mediated anti-inflammatory response induced by LPS, BMDM with *Nlrp3* knockout (*Nlrp3*<sup>-/-</sup> BMDM) was used. Deletion of *Nlrp3* largely abrogated the GPA-mediated reduction of genes expression (e.g. *Nf $\kappa$ b1*, *IL-1 $\beta$*  and *IL-6*) and the cytokines generation (IL-1 $\beta$  and IL-6) in *Nlrp3*<sup>-/-</sup> BMDM (Fig. 2F and G), suggesting that these processes are dependent on NLRP3 suppression.

NF- $\kappa$ B can bind to the NLRP3 promoter region, thereby facilitating transcriptional regulation of LPS-induced NLRP3 gene expression [14, 15], suggesting that GPA-mediated NLRP3 inhibition might be likely by regulating NF- $\kappa$ B signaling. GPA pretreatment significantly inhibited the NF- $\kappa$ B-luc promoter luciferase activity and we also observed a strong inhibitory effect on NF- $\kappa$ B-luc activity by GPA pretreatment prior to LPS stimulation (Fig. 2H). Furthermore, LPS stimulation induced translocation of NF- $\kappa$ B p65 from cytoplasmic to nuclear in THP-1 cells, which was inhibited by GPA pretreatment prior to LPS stimulation (Fig. 2I), and consequently resulting in an obvious decreases in the NLRP3 and ASC protein levels (Fig. 2J) and pro-inflammatory genes expression (Fig. 2A). Collectively, our results demonstrated that GPA represses NLRP3 expression via regulation of NF- $\kappa$ B activation.

### 2.3. GPA suppresses NLRP3 inflammasome activation

Sufficient NLRP3 protein levels are crucial for the formation and activation of NLRP3 inflammasome [16,17]. Considering that GPA

inhibited NLRP3 activity, we determined whether GPA could block NLRP3 inflammasome activation. As shown in Fig. 3 A, GPA pretreatment of LPS-primed THP-1 cells prior to NLRP3 activation using ATP resulted in reduced secretion of IL-1 $\beta$ , TNF- $\alpha$ , and IL-6. The effect of GPA



(caption on next page)

**Fig. 1. GPA directly binds to NLRP3 and represses its expression.** (A) Dual-luciferase reporter assay results. RAW264.7 cells were transiently co-transfected with NLRP3-luc plasmids for 12 h and treated with DMSO (vehicle control), GPA-H (100  $\mu$ M), GPA-M (50  $\mu$ M), GPA-L (25  $\mu$ M), or MCC950 (10  $\mu$ M) for 24 h. Relative luciferase activity was calculated by ration of firefly luciferase/renilla luciferase activity ( $n = 5$ ). \* $P < 0.05$ , \*\* $P < 0.01$ , compared to the DMSO control transfected with empty vector. Data are expressed as the mean  $\pm$  SEM of 5 independent experiments ( $n = 5$ ). (B) mRNA levels of *NLRP3*, *NF $\kappa$ B1*, and *IL-1 $\beta$*  in THP-1 monocyte-derived macrophages and BMDM as analyzed by real-time PCR after 24 h treatment with different concentrations of GPA (25–100  $\mu$ M). Results are expression as fold changes compared to the DMSO group. Data are expressed as the mean  $\pm$  SEM of 5 independent experiments ( $n = 5$ ). \* $P < 0.05$ , \*\* $P < 0.01$  versus DMSO control group. (C) Protein levels of NLRP3, ASC, CASP-1, and IL-1 $\beta$  in THP-1 monocyte-derived macrophages were determined by Western blot analysis after 24 h treatment with different concentrations of GPA.  $\beta$ -ACTIN was used as internal reference protein. Data are expressed as the mean  $\pm$  SEM of 3 independent experiments ( $n = 3$ ). (D) Cell lysates of LPS-primed THP-1 monocytes were incubated with GPA (100  $\mu$ M) or Bio-GPA (100  $\mu$ M) for 4 h and subjected to pull-down assays with streptavidin beads. Total (input), bound (pull-down), and remaining proteins (after pull-down) were immunoblotted as indicated.  $\beta$ -ACTIN was used as internal reference protein. Data are expressed as the mean  $\pm$  SEM of 3–4 independent experiments ( $n = 3–4$ ). (E) Competitive experiment. Cell lysates of LPS-primed THP-1 monocytes were incubated with Bio-GPA (100  $\mu$ M) and different concentrations of free GPA (50 or 100  $\mu$ M) and subjected to pull-down assays with streptavidin beads.  $\beta$ -ACTIN was used as internal reference protein. Data are expressed as the mean  $\pm$  SEM of 3–4 independent experiments ( $n = 3–4$ ). (F) Human recombinant NLRP3 proteins were incubated with the indicated doses of Bio-GPA (50 or 100  $\mu$ M) and subjected to pull-down assays with streptavidin beads. NLRP3 was used as internal reference protein. Data are expressed as the mean  $\pm$  SEM of 3–4 independent experiments ( $n = 3–4$ ). (G) Human recombinant NLRP3 proteins were incubated with Bio-GPA (100  $\mu$ M) or/and  $\beta$ -Mercaptoethanol (50  $\mu$ M) and subjected to pull-down assays with streptavidin beads. NLRP3 was used as internal reference protein. Data are expressed as the mean  $\pm$  SEM of 3–4 independent repeats ( $n = 3–4$ ).

was further confirmed by Western blot as GPA could block the cleavage of IL-1 $\beta$  and CASP-1 to their mature p17 and p20 forms, respectively, by directly reducing NLRP3 and ASC at protein (Fig. 3B and Fig. S3A). In parallel, the mRNA expression levels of pro-inflammatory genes including NLRP3, NF $\kappa$ B1, IL-1 $\beta$ , IL-6, ICAM-1 and TNF- $\alpha$  were also reduced by GPA pretreatment and GPA pretreatment inhibits LPS + ATP-induced nuclear translocation of NF- $\kappa$ Bp65 (Fig. 3C and Fig. S3B). Similar results were observed in BMDM, as shown by the inhibition of NLRP3-mediated pro-inflammatory gene expression and cytokines production (Figs. S3C and D). However, the GPA-mediated repression of pro-inflammatory gene expression (*Nf $\kappa$ b1*, *IL-1 $\beta$* , *IL-6*, *Icam-1*, *Tnf- $\alpha$*  and *Cox-2*) and cytokines release (IL-1 $\beta$  and IL-6) were partially abolished in LPS + ATP-induced *Nlrp3*<sup>-/-</sup> BMDM (Figs. S3E and F).

One essential step for NLRP3 inflammasome activation is the recruitment of ASC to NLRP3 oligomers for assembly complex [18]. Next, we determined whether GPA could inhibit the generation of NLRP3 inflammasome complex. Indeed, we found that GPA pretreatment could suppress LPS + ATP-induced endogenous NLRP3–ASC interaction in THP-1 cells (Fig. 3D). Mechanically, pretreatment of THP-1 cells with GPA significantly reduced LPS + ATP-induced ROS generation (Fig. 3E) and altered intracellular K<sup>+</sup>/Ca<sup>2+</sup> fluxes (Fig. 3F and G), the proposed upstream signaling events involved in NLRP3 activation [19,20]. A similar decrease of ROS generation was also observed in BMDM cells (Fig. S3G). Thus, we showed that GPA blocked NLRP3 inflammasome activation mainly by directly regulating signals 1 and 2 via the suppression of ROS generation and intracellular ion fluxes.

#### 2.4. GPA alleviates ANIT- and LPS-induced acute cholestatic liver injury by suppressing NLRP3 inflammasome activation

Previously, GPA has been reported to protect against various chemical hepatotoxicants, including ANIT- and GalN/LPS-induced hepatotoxicity [21]. However, whether GPA can alleviate ANIT- or LPS-induced acute cholestatic liver inflammation and the underlying molecular mechanism remain uninvestigated. BAs can synergize with LPS and ATP to activate the NLRP3 inflammasome, thereby amplifying the hyperinflammatory responses in the early phase of sepsis [22]. As GPA can inhibit NLRP3 inflammasome, we speculate that GPA may alleviate ANIT- or LPS-induced acute cholestatic liver inflammation via the inhibition of NLRP3 inflammasome. As expected, GPA pretreatment effectively improved ANIT-induced cholestatic liver injury as evidenced by decreased liver weight index, serum levels of biochemical parameters, including ALT, AST, TBA, and TBIL (Fig. S4A). Liver histopathological changes induced by ANIT were associated with the damaged lobular structure, watery degeneration of hepatocytes, as well as necrosis, and accompanied by a visible bleeding in ANIT-treated mice compared with control-treated mice. However, GPA pretreatment could prominently ameliorate such effects (Figs. S4B–D). Importantly, FACS

analysis of F4/80 and CD11b and immunofluorescence analysis of F4/80 and CD68 demonstrated that inflammatory infiltration of liver tissues induced by ANIT was notably blunted by GPA pretreatment (Fig. 4A and B). Consistently, elevated liver inflammation was reversed by GPA pretreatment as evidenced by reduced cytokines levels including IL-1 $\beta$ , TNF- $\alpha$ , and IL-6, and improved spleen weight index (Fig. 4C and D). Consistently, ANIT-induced NLRP3 inflammasome activation was reversed by GPA pretreatment, as evidenced by decreased NLRP3, ASC, CASP-1, and IL-1 $\beta$  at both the protein and mRNA levels (Fig. 4E and F and Fig. S4E). GPA also diminished the ANIT-induced elevation of phosphorylated NF- $\kappa$ B p65 and phosphorylated I $\kappa$ B $\alpha$  levels via increasing I $\kappa$ B $\alpha$  levels, leading to reduced pro-inflammatory genes expression (*IL-6*, *Icam-1*, and *Cox-2*) in the liver (Fig. 4E and F and Fig. S4E). Of note, in accordance with the reduced LPS + ATP-induced ROS generation in THP-1 cells, GPA pretreatment also prominently mitigated ANIT-induced ROS generation in cholestatic liver tissues (Fig. 4G).

Excessive inflammation restrains BA transport and synthesis via regulation of genes involved in BA transport and synthesis during acute cholestatic liver inflammation [20], thereby aggravating the retention of BAs in the liver. Thus, we determined whether GPA pretreatment contributes to restore hepatic BA homeostasis. As expected, we found that ANIT-induced acute cholestatic liver inflammation significantly suppressed the expression of genes involved in BA synthesis (including *Cyp7a1* and *Cyp27a1*), excretion (*Abcb11*, *Abcc2*, *Abcc3*, and *Abcc4*), uptake (*Slc10a1* and *Slc01b2*), and BA-detoxifying enzymes (*Cyp3a11*, *Cyp2b10*, and *Ugt1a1*) (Fig. 5A), resulting in excessive accumulation of BAs in the liver (Fig. 5B) and subsequently inducing liver inflammation. However, the phenomenon was partly reversed by GPA pretreatment (e. g., upregulation of *Abcb11*, *Abcc2*, *Abcc3*, *Abcc4* and *Ugt1a1*), thereby reducing liver BA levels, especially those taurine-conjugated BAs (e. g., TCA).

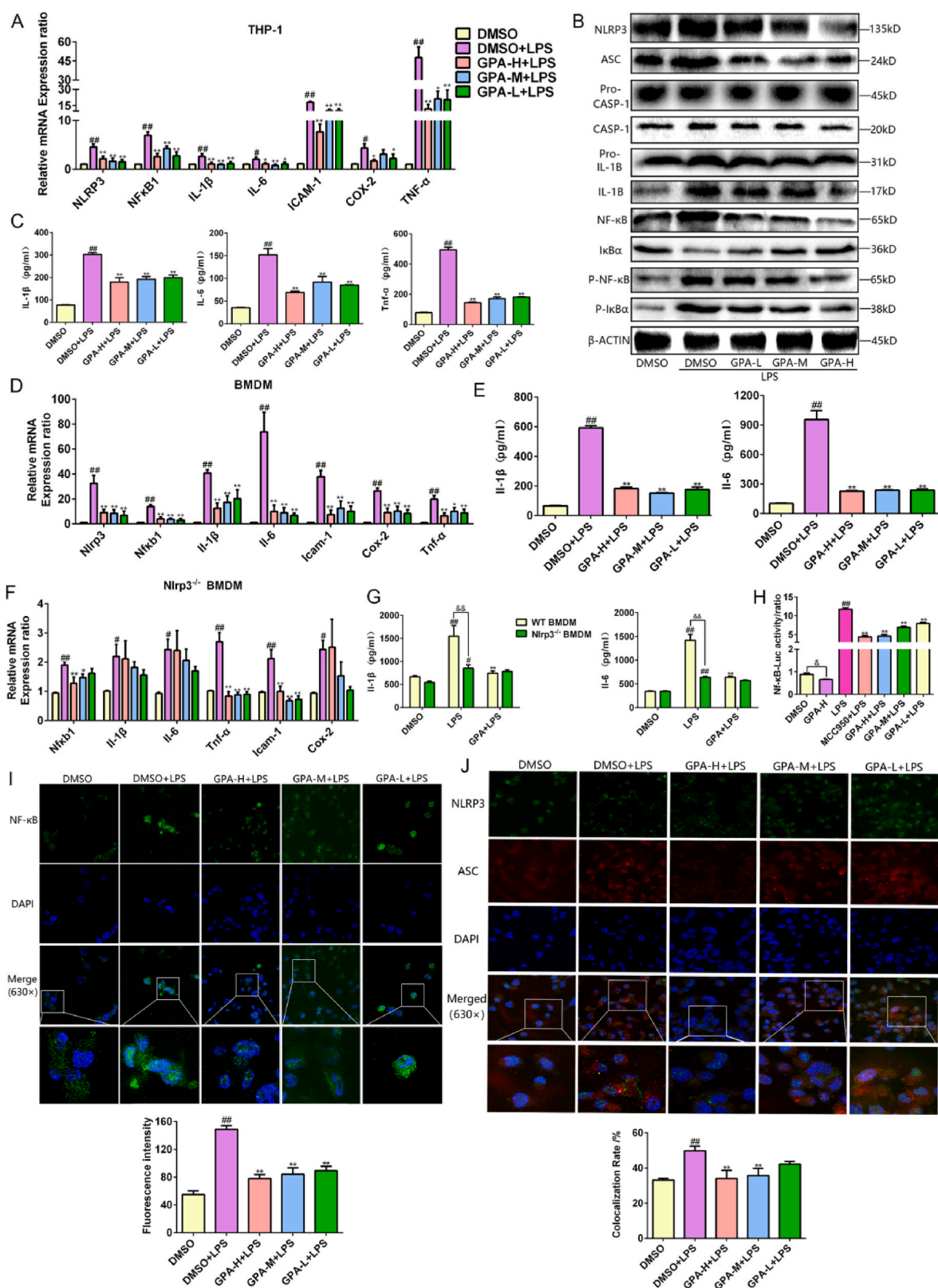
Clinically, cholestasis is a common complication in patients with extrahepatic infections and sepsis [23]. To further validate the protective effect of GPA against cholestatic liver inflammation, we established an LPS-induced septic cholestasis in mice. We observed that GPA pretreatment significantly diminishes LPS-induced septic cholestatic inflammation as evidenced by decreased serum levels of ALT, AST, TBA, TBIL, IL-1 $\beta$ , and IL-6 levels, subsequently leading to an overall liver histopathological improvement (Fig. S5). Collectively, our results indicate that GPA could ameliorate acute cholestatic liver inflammation by inhibiting NF- $\kappa$ B and NLRP3 inflammasome activation.

#### 2.5. NLRP3 inflammasome activation enhances mutual crosstalk between hepatocytes and macrophages to exacerbate BA-induced hepatocyte inflammation

BAs can directly injure liver cells in cholestatic liver disease by

initiating a cytokine-mediated inflammatory response [9,24], suggesting that BA-induced inflammation exacerbates liver injury during cholestasis. Therefore, the control of hepatocyte inflammation represents a potent therapeutic strategy for the treatment of early-phase cholestatic liver injury. To investigate whether GPA can alleviate

BA-induced hepatocyte inflammatory injury by suppressing NLRP3 inflammasome activation, we isolated primary mouse hepatocytes (PMHs) and treated them with GPA prior to BA induction. Upon pre-treatment with 200  $\mu$ M TCA, the major endogenous BA whose concentration varies highly between 100 and 300  $\mu$ M in cholestatic mice for 24



(caption on next page)

**Fig. 2. GPA reduces LPS-induced NLRP3 expression via inhibiting NF- $\kappa$ B signaling.** (A–C) THP-1 monocytes were pretreated with the indicated concentrations of GPA for 24 h and stimulated with LPS (1  $\mu$ g/ml) for 24 h. The levels of mRNA (A), protein (B), and pro-inflammatory cytokines in supernatants (C) were measured by real-time PCR, Western blot, and ELISA, respectively. mRNA results are expressed as fold changes compared to the DMSO group.  $\beta$ -ACTIN was used as internal reference protein. Data are expressed as the mean  $\pm$  SEM of 3–5 independent experiments ( $n = 5$ , A and C;  $n = 3$ , B). \* $P < 0.05$ , \*\* $P < 0.01$  versus DMSO-treated control group, \* $P < 0.05$ , \*\* $P < 0.01$  versus LPS-treated group. (D–E) BMDM were pretreated with indicated concentrations of GPA for 24 h and stimulated with LPS (1  $\mu$ g/ml) for 24 h. The levels of mRNA (D) and pro-inflammatory cytokines in supernatants (E) were determined by real-time PCR and ELISA, respectively. mRNA results are expressed as fold changes compared to the DMSO group. Data are expressed as the mean  $\pm$  SEM of 5 independent experiments ( $n = 5$ ). \* $P < 0.05$ , \*\* $P < 0.01$  versus DMSO-treated control group, \* $P < 0.05$ , \*\* $P < 0.01$  versus LPS-treated group. (F and G) *Nlrp3*<sup>-/-</sup> BMDM were pretreated with indicated concentrations of GPA for 24 h and stimulated with LPS (1  $\mu$ g/ml) for 24 h. The levels of mRNA (F) and pro-inflammatory cytokines in supernatants (G) were determined by real-time PCR and ELISA, respectively. mRNA results are expressed as fold changes compared to the DMSO group. Data are expressed as the mean  $\pm$  SEM of 5 independent experiments ( $n = 5$ ). \* $P < 0.05$ , \*\* $P < 0.01$  versus DMSO-treated control group, \* $P < 0.05$ , \*\* $P < 0.01$  versus LPS-treated group. (H) Dual-luciferase reporter assay results. RAW274.6 cells were transiently co-transfected with NF- $\kappa$ B-luc plasmids for 12 h and treated with DMSO (vehicle control), GPA-H (100  $\mu$ M), GPA-M (50  $\mu$ M), GPA-L (25  $\mu$ M), or MCC950 (10  $\mu$ M) for 12 h, followed by 24 h induction with LPS (1  $\mu$ g/ml). Data are expressed as the mean  $\pm$  SEM of 5 independent experiments ( $n = 5$ ). (I and J) The protein expression levels of NF- $\kappa$ B (I), NLRP3 and ASC (J) in THP-1 monocytes were measured by immunofluorescence assay. The nuclei were stained with DAPI in blue, and targeted protein was stained in green or red (magnification: 630  $\times$ ). (For interpretation of the references to colour in this figure legend, the reader is referred to the Web version of this article.)

h, the genes expression of *Nlrp3* and *Nfkb1* were dramatically elevated, accompanied with increased levels of pro-inflammatory genes including that of *Il-1 $\beta$* , *Il-6*, *Icam-1*, *Cox-2*, and *Tnf- $\alpha$* , which were largely abrogated by GPA/MCC950-mediated NLRP3 inhibition (Fig. 6A), resulting in decreased *Il-1 $\beta$*  and *Tnf- $\alpha$*  generation (Fig. 6B). However, the inhibition of *Il-1 $\beta$*  expression and production by GPA was largely abolished in *Nlrp3*<sup>-/-</sup> PMHs (Fig. 6C and D), thereby demonstrating the critical role of NLRP3 in GPA-mediated protection against TCA-induced hepatocyte inflammation.

Activation of macrophages including liver-resident macrophages (Kupffer cells; KCs) and BMDMs, contributes to cholestatic liver injury [25,26]. During cholestatic liver injury, the deletion of KCs prevented Notch-mediated hepatocytes transformation to cholangiocytes [27], thus indicating that hepatocytes could communicate with macrophages via unknown mechanisms. BAs activate pro-inflammatory cytokine signaling in both hepatocytes and macrophages. However, the underlying mechanism of this crosstalk during BA-induced inflammatory injury remains largely unclear. To explore the underlying processes, we isolated PMHs and BMDM from WT and *Nlrp3*<sup>-/-</sup> mice and conducted on the conditional media (CM)-associated culture. Because the pathophysiological concentration of BAs induces the production of pro-inflammatory cytokines in mouse and human hepatocytes, but not in nonparenchymal cells and cholangiocytes [4], isolated BMDM from WT and *Nlrp3*<sup>-/-</sup> mice were exposed for 24 h to the CM of cultured WT-PMHs that were pretreated with GPA and/or TCA for 24 h each. According to real-time PCR analysis, the levels of pro-inflammatory mRNAs, including that of *Nlrp3*, *Nfkb1*, *Il-1 $\beta$* , *Il-6*, and *Tnf- $\alpha$* , were markedly decreased in BMDM exposed to the CM of WT-PMHs treated with both GPA and TCA compared with those with TCA alone (Fig. 6E and F). In contrast, this effect was partly abrogated in BMDM exposed to the CM of *Nlrp3*<sup>-/-</sup> PMHs treated with GPA and/or TCA (Fig. 6G and H). These results suggest that BA-induced proinflammatory cytokines release from PMHs activates liver macrophages to induce NLRP3 inflammasome activation and the effect is inhibited by GPA pretreatment via direct hepatic NLRP3 inhibition.

Subsequently, we detected a notable activation of NLRP3 and NF- $\kappa$ B signaling in TCA-treated BMDM, which was dramatically blunted by GPA and MCC950 pretreatment (Fig. 6I and J). In addition, the mRNA levels of *Nlrp3*, *Nfkb1*, *Il-1 $\beta$* , *Il-6*, and *Tnf- $\alpha$* , were notably decreased in PMHs exposed to the CM of WT-BMDM treated with GPA and TCA compared with those treated with TCA alone (Fig. 6K and L). This effect was largely blunted in PMHs exposed to the CM of *Nlrp3*<sup>-/-</sup> BMDM treated with GPA and/or TCA (Fig. 6M and N). Similar regulatory patterns were found in WT-PMHs and WT-BMDM (Fig. S6), which were exposed for 24 h to the CM collected from WT- and *Nlrp3*<sup>-/-</sup> BMDM and WT- and *Nlrp3*<sup>-/-</sup> PMHs, respectively, that were previously pretreated with or without GPA for 24 h, and then followed by TCA for 24 h. These data demonstrate that NLRP3 inflammasome activation in liver macrophages releases excessive pro-inflammatory cytokines and possibly

enhances the mutual crosstalk between hepatocytes and macrophages, leading to the augmentation of hepatocyte inflammation.

## 2.6. Repression of NLRP3 inflammasome activation is necessary for GPA-mediated hepatoprotective effect

To determine the role of NLRP3 in GPA-mediated hepatoprotection against ANIT-induced cholestatic liver inflammation, we generated mice with global deletion of *Nlrp3* (*Nlrp3*<sup>-/-</sup>) and those with liver *Nlrp3*-overexpression (*Nlrp3*<sup>oe</sup>) by infection with Adv-NLRP3 via tail vein injection. To a certain degree, the former displayed resistance to ANIT-induced cholestatic liver inflammatory injury compared to WT mice as evidenced by decreased inflammatory infiltration (Fig. 7A and B), suppressed the expression of inflammatory genes (*Nfkb1*, *Nlrp3*, *Il-1 $\beta$* , *Il-6*, *Tnf- $\alpha$* , *Icam-1*, and *Cox2*), and reduced the generation of cytokines (*Il-1 $\beta$* , *Il-6* and *Tnf- $\alpha$* ) (Fig. 7C–E), furthermore, significantly improved liver function (e.g. decreased ALT, AST, TBA, and TBIL levels) and less liver pathological lesions (e.g. decreased necrosis of hepatocytes, inflammation and tissue bleeding) were observed (Fig. 8A and B). *Nlrp3*<sup>-/-</sup> mice also had elevated genes expression of basolateral membrane transporters (*Abcc3*), and detoxifying enzymes (*Cyp3a11*) and reduced genes expression of bile-acid synthesis enzymes (*Cyp8b1* and *Cyp27a1*) and uptake transporter *Slc10a1* in comparison with WT mice (Fig. 8C). Surprisingly, a moderate decrease in the genes expression of apical membrane transporters, including *Abcb11* and *Abcc2*, was observed in *Nlrp3*<sup>-/-</sup> mice (Fig. 8A). These changes of *Nlrp3*<sup>-/-</sup> mice were associated with the low TBA and TBIL levels in the liver compared with WT mice (Fig. 8A). GPA pretreatment effectively mitigated ANIT-induced cholestatic liver inflammation via inhibiting inflammatory infiltration, and suppressing the expression of inflammatory genes (Fig. 7). In addition, increased BA efflux and detoxification were also observed in WT mice resulting in an obvious improvement of liver injury (Fig. 8). Conversely, GPA-mediated attenuation was partially impaired in *Nlrp3*<sup>-/-</sup> mice (Figs. 7 and 8). In addition, in *Nlrp3*<sup>oe</sup> mice, GPA-mediated hepatoprotective effects were also partially abated in comparison with the control mice (Fig. 9). Collectively, our data indicate that NLRP3 signaling plays an important role in the progression of cholestasis and GPA exerts hepatoprotective effects partially by inhibiting the activation of NLRP3 inflammasome.

## 2.7. Disruption of mutual crosstalk between hepatocytes and liver macrophages dampens GPA-mediated hepatoprotective effect

Liver overexpression of *Nlrp3* (*Nlrp3*<sup>oe</sup>) may intensify the crosstalk between hepatocytes and liver macrophages, resulting in the mitigation of the hepatoprotective effect of GPA. We investigated whether the disruption of this communication dampens GPA-mediated hepatoprotection against ANIT-induced cholestatic liver inflammation in a mouse model with consumption of macrophages. Following the

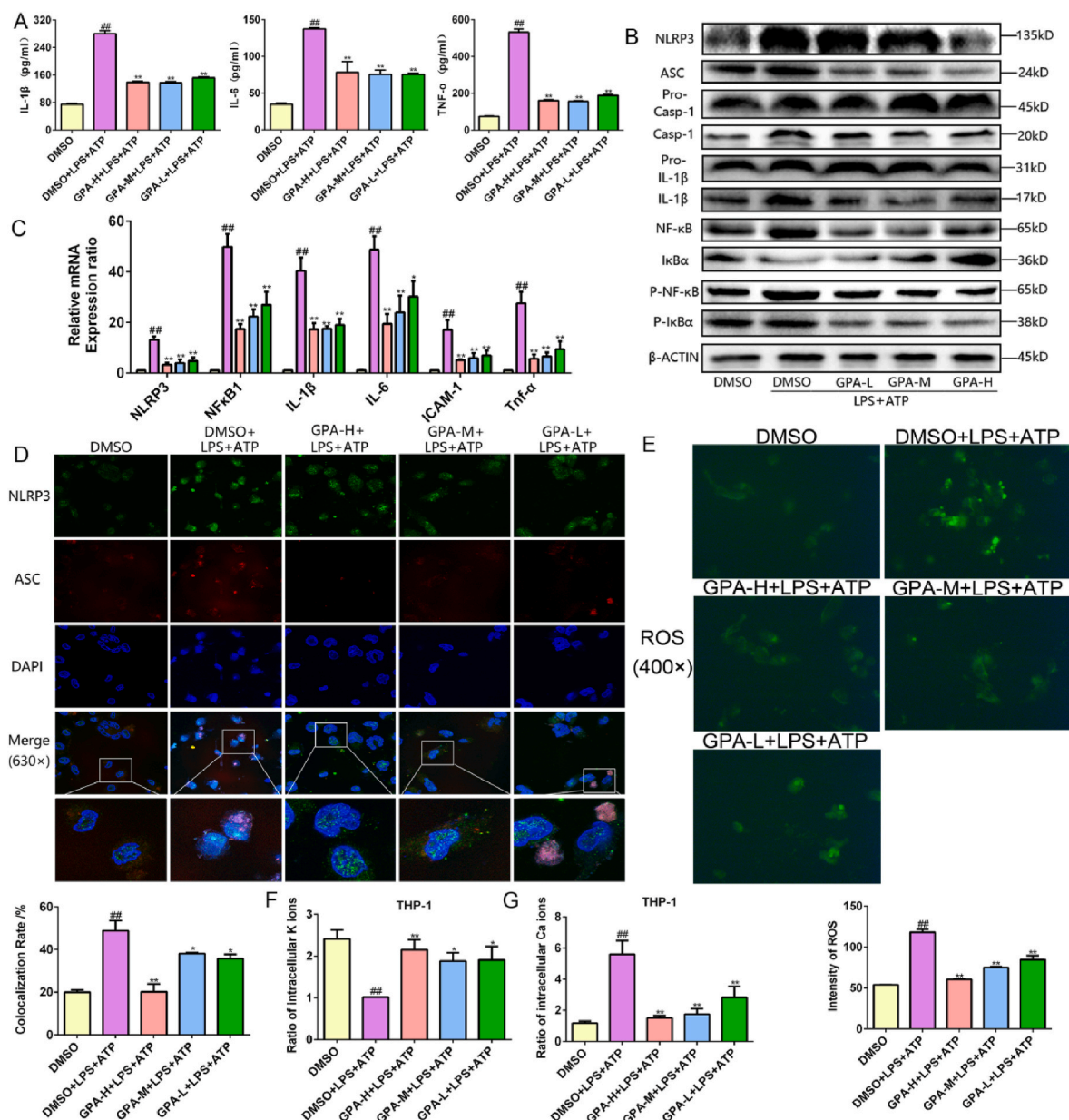


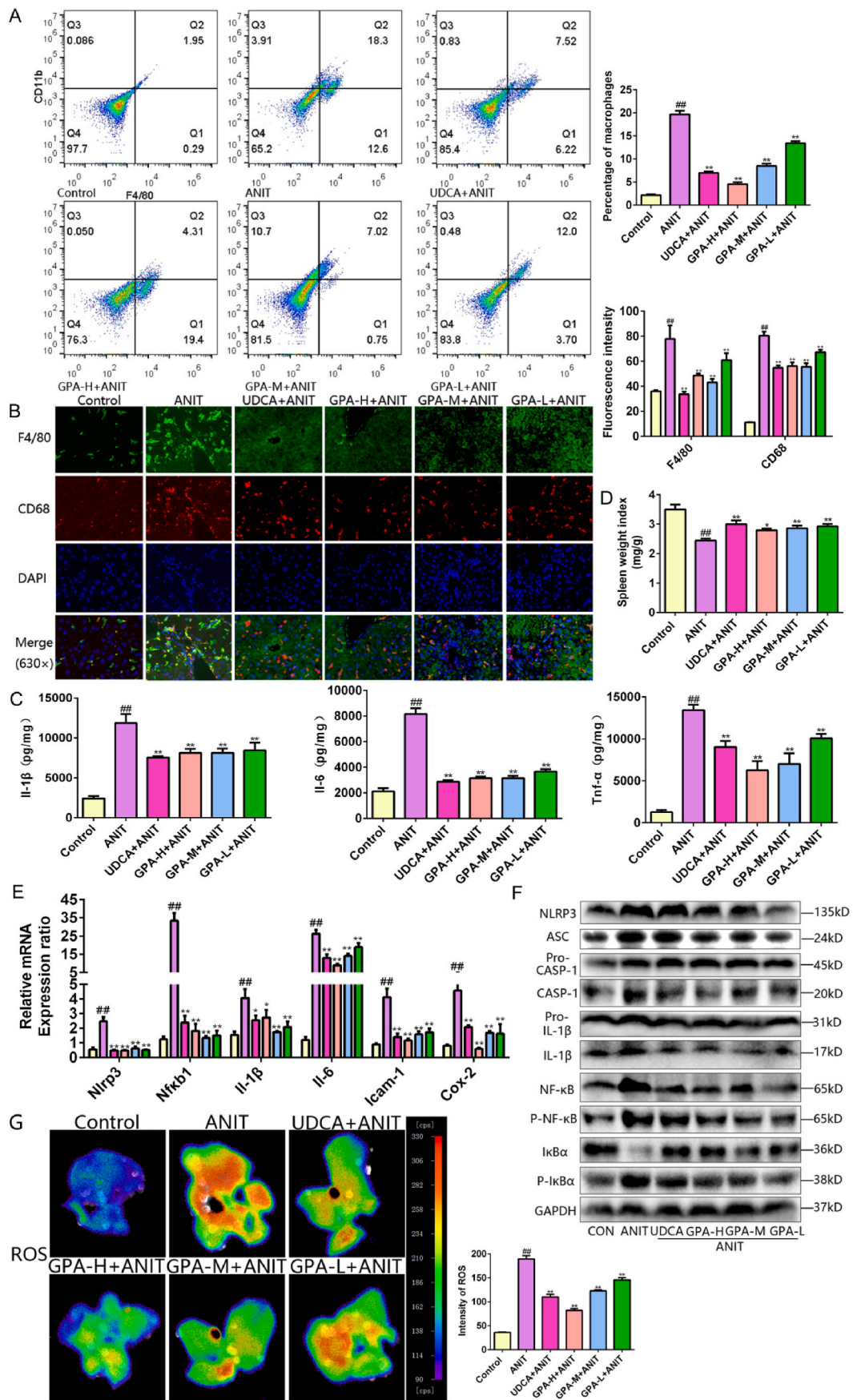
**Fig. 3. GPA suppresses NLRP3 inflammasome activation.** (A–C) THP-1 monocytes were pretreated with indicated concentrations of GPA for 24 h, stimulated with LPS (1  $\mu$ g/ml) for 24 h and ATP (2.5 mM) for 30 min. (A) The levels of pro-inflammatory cytokines in cell-culture supernatants, including IL-1 $\beta$ , IL-6, and TNF- $\alpha$  were quantified by ELISA. Data are expressed as the mean  $\pm$  SEM of 5 independent experiments ( $n = 5$ ). The levels of protein (B) and mRNA (C) were determined by Western blot analysis and real-time PCR, respectively. mRNA results are expressed as fold changes compared to the DMSO group.  $\beta$ -ACTIN was used as internal reference protein. Data are expressed as the mean  $\pm$  SEM of 3–5 independent experiments ( $n = 3$ –4, B;  $n = 5$ , C).  $^{\#}P < 0.05$ ,  $^{\#\#}P < 0.01$  versus DMSO-treated control group,  $^*P < 0.05$ ,  $^{**}P < 0.01$  versus LPS + ATP-treated group. (D) The NLRP3-ASC interaction in THP-1 monocytes were measured by immuno-fluorescence assay. The nuclei were stained with DAPI in blue, and targeted protein was stained in green or red (magnification:  $630 \times$ ). (E) ROS levels were detected using an ROS fluorescent probe in THP-1 monocytes (magnification:  $400 \times$ ). (F and G) Intracellular potassium (F) and ionic calcium (G) levels in the cell lysates of THP-1 monocytes. Data are expressed as the mean  $\pm$  SEM of 5 independent experiments ( $n = 5$ ).  $^{\#}P < 0.05$ ,  $^{\#\#}P < 0.01$  versus DMSO-treated control group,  $^*P < 0.05$ ,  $^{**}P < 0.01$  versus LPS + ATP-treated group. (For interpretation of the references to colour in this figure legend, the reader is referred to the Web version of this article.)

injection of liposomal clodronate [27,28], we observed partial hepatoprotection as evidenced by the decreased ALT levels in the serum (Fig. 10 A) and TBA and TBIL levels in both serum and liver (Fig. 10 B), diminished inflammation infiltration (Fig. 10C–E) and improved liver histopathological injury (Fig. 10F) compared with the control group. GPA-mediated NLRP3 inhibition effectively ameliorated ANIT-induced cholestatic liver inflammation in the control mice with intact liver macrophages (Fig. 10); however, this effect was partially weakened in liposomal clodronate-treated mice. Collectively, these results confirm

that NLRP3-mediated the mutual crosstalk between hepatocytes and liver macrophages plays a critical role in GPA-mediated hepatoprotective effect against ANIT-induced cholestatic liver inflammation.

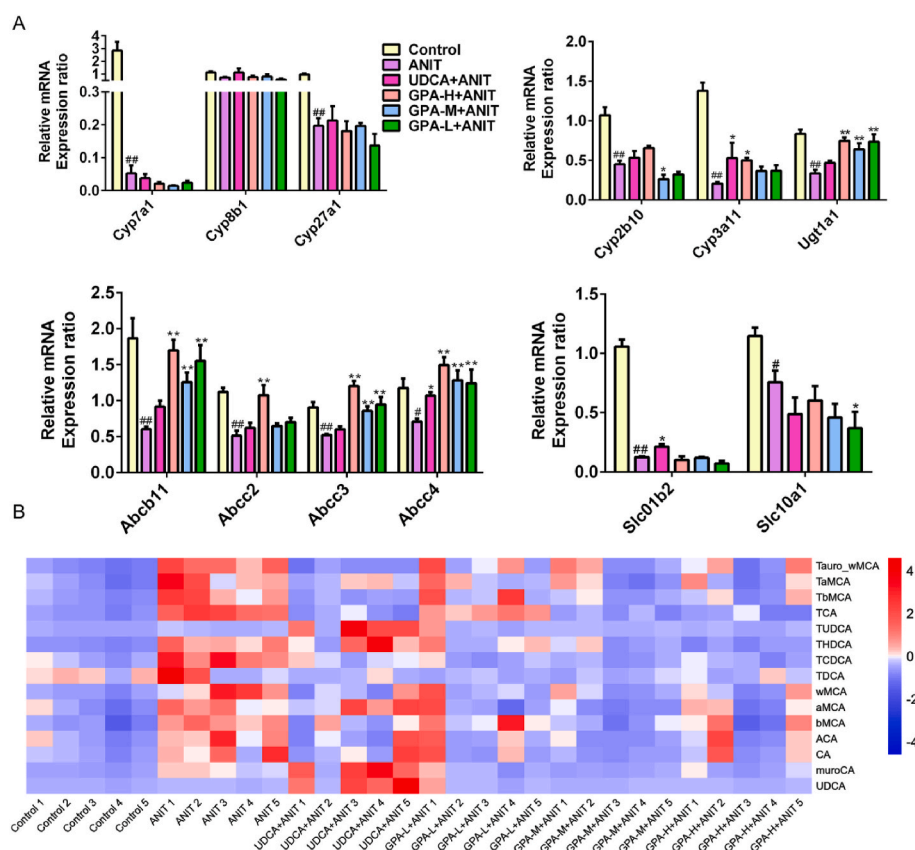
### 3. Discussion

In the current study, we revealed that GPA could act as a specific inhibitor of NLRP3 inflammasome activation in mice with cholestasis



(caption on next page)

**Fig. 4. GPA protects against ANIT-induced acute liver inflammation by inhibiting NLRP3 inflammasome activation.** C57BL/6 mice were orally administered with the vehicle (0.5% carboxymethylcellulose) as control group, UDCA (75 mg/kg) as positive control, GPA-H (100 mg/kg), GPA-M (50 mg/kg), or GPA-L (25 mg/kg) daily for seven days. On day 5, they were orally administered with ANIT (100 mg/kg). (A) Representative FACS image of mouse liver sample. After sacrificing the animals, liver macrophage were isolated, and the inflammatory infiltration was evaluated by FACS ( $n = 5$ ). Data are expressed as the mean  $\pm$  SEM of 5 independent mice liver samples ( $n = 5$ ).  $^{\#}P < 0.05$ ,  $^{\#\#}P < 0.01$  versus vehicle-treated control group,  $^*P < 0.05$ ,  $^{**}P < 0.01$  versus ANIT-treated group. (B) Hepatic F4/80 and CD68 protein expression measured by immunofluorescence assay. The nuclei were stained with DAPI in blue, and targeted protein was stained in green (F4/80) or red (CD68) (magnification:  $630 \times$ ). (C) Levels of pro-inflammatory cytokines in mouse liver, including IL-1 $\beta$ , IL-6, and Tnf- $\alpha$  were detected by ELISA. Data are expressed as the mean  $\pm$  SEM of 5–6 independent mouse samples ( $n = 5$ –6).  $^{\#}P < 0.05$ ,  $^{\#\#}P < 0.01$  versus vehicle-treated control group,  $^*P < 0.05$ ,  $^{**}P < 0.01$  versus ANIT-treated group. (D) Changes in spleen weight index (ratio of spleen weight to body weight) in mice with ANIT-induced cholestasis. Data are expressed as the mean  $\pm$  SEM of 5 independent mouse samples ( $n = 5$ ). (E) mRNAs levels of NLRP3 and other proinflammatory genes in mouse liver were analyzed by real-time PCR. Data are expressed as the mean  $\pm$  SEM of 5 independent mouse samples ( $n = 5$ ). Results are expressed as fold changes compared to the vehicle-treated control group.  $^{\#}P < 0.05$ ,  $^{\#\#}P < 0.01$  versus vehicle-treated control group,  $^*P < 0.05$ ,  $^{**}P < 0.01$  versus ANIT-treated group. (F) Levels of NLRP3 and NF- $\kappa$ B signaling proteins in liver lysates were analyzed by western blotting.  $\beta$ -ACTIN was used as internal reference protein. Data are expressed as the mean  $\pm$  SEM of 3–4 independent mouse samples ( $n = 3$ –4).  $^{\#}P < 0.05$ ,  $^{\#\#}P < 0.01$  versus vehicle-treated control group,  $^*P < 0.05$ ,  $^{**}P < 0.01$  versus ANIT-treated group. (G) ANIT-induced hepatic ROS levels were decreased after GPA treatment ( $n = 3$ ).  $^{\#}P < 0.05$ ,  $^{\#\#}P < 0.01$  versus vehicle-treated control group,  $^*P < 0.05$ ,  $^{**}P < 0.01$  versus ANIT-treated group. (For interpretation of the references to colour in this figure legend, the reader is referred to the Web version of this article.)

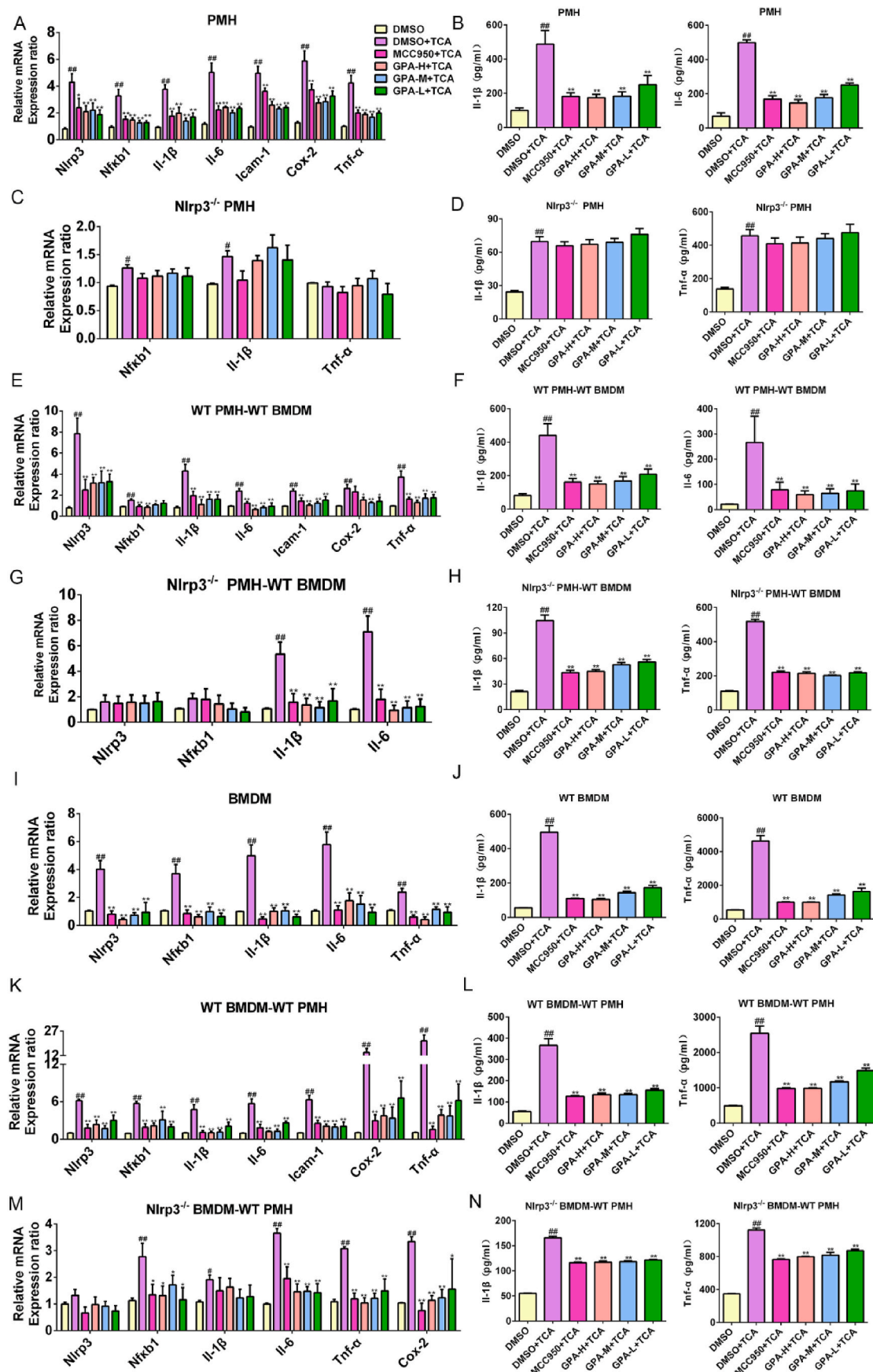


and macrophage cells *in vitro*. GPA covalently binds to NLRP3 and inhibits NLRP3 activation by regulating the crosstalk between hepatocytes and liver macrophages. More specifically, GPA effectively attenuated ANIT-induced NLRP3 inflammasome-dependent cholestatic liver inflammation in mice. Overall, our findings provide new insights on the potential application of GPA for the treatment of NLRP3 inflammasome-related diseases, such as cholestasis.

Many molecules, including sulforaphane,  $\beta$ -hydroxybutyrate (BHB), flufenamic acid, CY-09, parthenolide, BAY 11-7082, INF39, and MCC950 have shown potent inhibitory effects on NLRP3 activation and have been tested extensively in animal models; however, their nonspecific effects have limited their clinical potential. For instance, sulforaphane also inhibited the activity of the AIM2 and NLRC4 inflammasomes and the activation of NF- $\kappa$ B; thus, its use could impair the role of these two inflammasomes in host defense [29]. Flufenamic acid and BHB regulated chloride and potassium efflux, respectively, they

could target the upstream signaling event of NLRP3 activation and may have undesired biological activities [25,30]. BAY11-7082 and INF39 have been reported to repress NLRP3 activation by directly inhibiting NLRP3 ATPase activity; such inhibitors have specific roles [26,31,32]. Therefore, inhibitory reagents that specifically act on the NLRP3 inflammasome itself, rather than upstream or downstream events of its activation, are the optimal choice for the treatment of NLRP3 inflammasome-associated diseases. However, to date, only a few of these compounds, including OLT1177, MCC950, CY-09, and oridonin, have been identified [33,34]. Here, we demonstrate that GPA is a specific inhibitor of NLRP3 inflammasome activation by covalently binding to NLRP3.

Our results also revealed the complex mechanism underlying this inhibitory effect. First, we found that GPA downregulated NLRP3 and pro-IL-1 $\beta$  expression by repressing NF- $\kappa$ B expression and its translocation to the nucleus, resulting in decreased production of cytokines,



(caption on next page)

**Fig. 6. GPA reduces BA-induced cellular inflammation by blocking the activation of NLRP3 inflammasome in hepatocytes and macrophages.** (A) Wild-type primary (WT) mouse hepatocytes (PMHs) were pretreated with GPA for 12 h and treated with 200  $\mu$ M TCA for 24 h. Levels of NLRP3 and proinflammatory mRNAs were determined by real-time PCR. Results are expression as fold changes compared to the DMSO group. Data are expressed as the mean  $\pm$  SEM of 5 independent experiments ( $n = 5$ ). (B) Levels of IL-1 $\beta$  and IL-6 in cell-culture supernatants were quantified by ELISA. Data are expressed as the mean  $\pm$  SEM of 5 independent experiments ( $n = 5$ ). \* $P < 0.05$ , \*\* $P < 0.01$  versus DMSO-treated control group, \* $P < 0.05$ , \*\* $P < 0.01$  versus TCA-treated group. Primary mouse hepatocytes with *Nlrp3*-knockout (*Nlrp3*<sup>-/-</sup>PMHs) were pretreated with GPA for 12 h and treated with 200  $\mu$ M TCA for 24 h. Levels of *Nfkb1*, *Il-1 $\beta$* , and *Tnf- $\alpha$*  mRNA (C) and IL-1 $\beta$  and *Tnf- $\alpha$*  in cell-culture supernatants (D) were determined by real-time PCR and ELISA, respectively. mRNA results are expression as fold changes compared to the DMSO group. Data are expressed as the mean  $\pm$  SEM of 5 independent experiments ( $n = 5$ ). \* $P < 0.05$ , \*\* $P < 0.01$  versus DMSO-treated control group, \* $P < 0.05$ , \*\* $P < 0.01$  versus TCA-treated group. PMHs and BMDM were isolated from WT and *Nlrp3*<sup>-/-</sup> mice and cultivated on a conditioned medium (CM)-associated culture. (E–H) WT BMDM were exposed for 24 h to the CM derived from WT-PMHs (E and F) and *Nlrp3*<sup>-/-</sup> PMHs (G and H) that were pretreated with or without GPA for 24 h and TCA for another 24 h. Levels of NLRP3 and proinflammatory mRNAs (E and G) and IL-1 $\beta$  (F and H) in cell-culture supernatants were determined by real-time PCR and ELISA, respectively. mRNA results are expressed as fold changes compared to the DMSO group. Data are expressed as the mean  $\pm$  SEM of 5 independent experiments ( $n = 5$ ). \* $P < 0.05$ , \*\* $P < 0.01$  versus DMSO-treated control group, \* $P < 0.05$ , \*\* $P < 0.01$  versus TCA-treated group. (I–J) BMDM were pretreated with GPA for 12 h and treated with 200  $\mu$ M TCA for 24 h. Levels of NLRP3 and proinflammatory mRNAs and pro-inflammatory cytokines in cell-culture supernatants were quantified by real-time PCR (I) and ELISA analysis (J), respectively. mRNA results are expressed as fold changes compared to the DMSO group. Data are expressed as the mean  $\pm$  SEM of 5 independent experiments ( $n = 5$ ). \* $P < 0.05$ , \*\* $P < 0.01$  versus DMSO-treated control group, \* $P < 0.05$ , \*\* $P < 0.01$  versus TCA-treated group. (K–N) WT PMHs were exposed for 24 h to the CM derived from WT-BMDM (K and L) and *Nlrp3*<sup>-/-</sup> (M and N) BMDM that were pretreated with or without GPA for 24 h, followed by TCA for 24 h. Levels of NLRP3 and proinflammatory mRNAs (K and M) and IL-1 $\beta$  (L and N) in cell-culture supernatants were determined by real-time PCR and ELISA analysis, respectively. mRNA results are expressed as fold changes compared to the DMSO group. Data are expressed as the mean  $\pm$  SEM of 5 independent experiments ( $n = 5$ ). \* $P < 0.05$ , \*\* $P < 0.01$  versus DMSO-treated control group, \* $P < 0.05$ , \*\* $P < 0.01$  versus TCA-treated group.

including inflammasome-dependent IL-1 $\beta$  and inflammasome-independent TNF- $\alpha$  and IL-6. *Nlrp3*-deletion partially abated GPA-mediated inhibition of pro-inflammatory cytokine production. This further supports the involvement of GPA-mediated NLRP3 inhibition in the priming step as NLRP3 is necessary for NF- $\kappa$ B-mediated induction of pro-IL-1 $\beta$  expression.

Second, the observed inhibitory effect on priming was not as strong as the inhibitory effect on NLRP3 inflammasome activation. Therefore, we explored the underlying mechanism of GPA inhibition. Initially, we validated its inhibitory effect on NLRP3 inflammasome activation induced by LPS + ATP. Then, we investigated the role of GPA on the upstream signals of NLRP3 inflammasome activation. ROS generation contributes to the activation of the NLRP3 inflammasome [55]. Our results showed that GPA suppressed ROS production during LPS + ATP-induced NLRP3 inflammasome activation. Numerous NLRP3 inflammasome activators, including ATP, neigericin, and crystalline, induce K<sup>+</sup> efflux, and intracellular K<sup>+</sup> reduction is an upstream event in the NLRP3 inflammasome activation [35]. Indeed, the interaction between NLRP3 and NEK7 is essential for NLRP3 inflammasome assembly and requires K<sup>+</sup> efflux [36]. Meanwhile, Ca<sup>2+</sup> signaling is necessary for NLRP3 activation, and the inhibition of Ca<sup>2+</sup> mobilization decreased NLRP3 activation [37]. Similarly, we found that GPA-mediated inhibition of NLRP3 activation is associated with the regulation of Ca<sup>2+</sup> and K<sup>+</sup> efflux signaling. Such results indicate that GPA has a notable effect on the upstream regulation of NLRP3 inflammasome activation. Next, we evaluated the role of GPA in inflammasome assembly and observed that GPA mitigated inflammasome assembly by blocking the interaction between NLRP3 and ASC, although the NLRP3–NEK7 interaction remains to be determined. Therefore, our results indicate that the interface between NLRP3 and ASC can be targeted to specifically inhibit NLRP3 inflammasome activation.

Based on its covalent inhibitors, including oridonin [13], and immunomodulatory metabolite itaconate [34], NLRP3 has been revealed as susceptible to electrophilic modification of reactive cysteines, thus implying a potential novel strategy for regulating the NLRP3 activation. Third, we identified the binding sites between GPA and NLRP3. Notably, GPA contains an  $\alpha,\beta$ -unsaturated carbonyl unit, which can covalently bind with the thiol of cysteine in the NACHT domain of NLRP3 via the Michael addition reaction to inhibit NLRP3 inflammasome activation. Consistently, pull-down assay results showed that the  $\beta$ -Me-mediated saturation of the C=C bond of bio-GPA abolished its association with NLRP3, highlighting the importance of the  $\alpha,\beta$ -unsaturated carbonyl group in inhibitory effect of GPA.

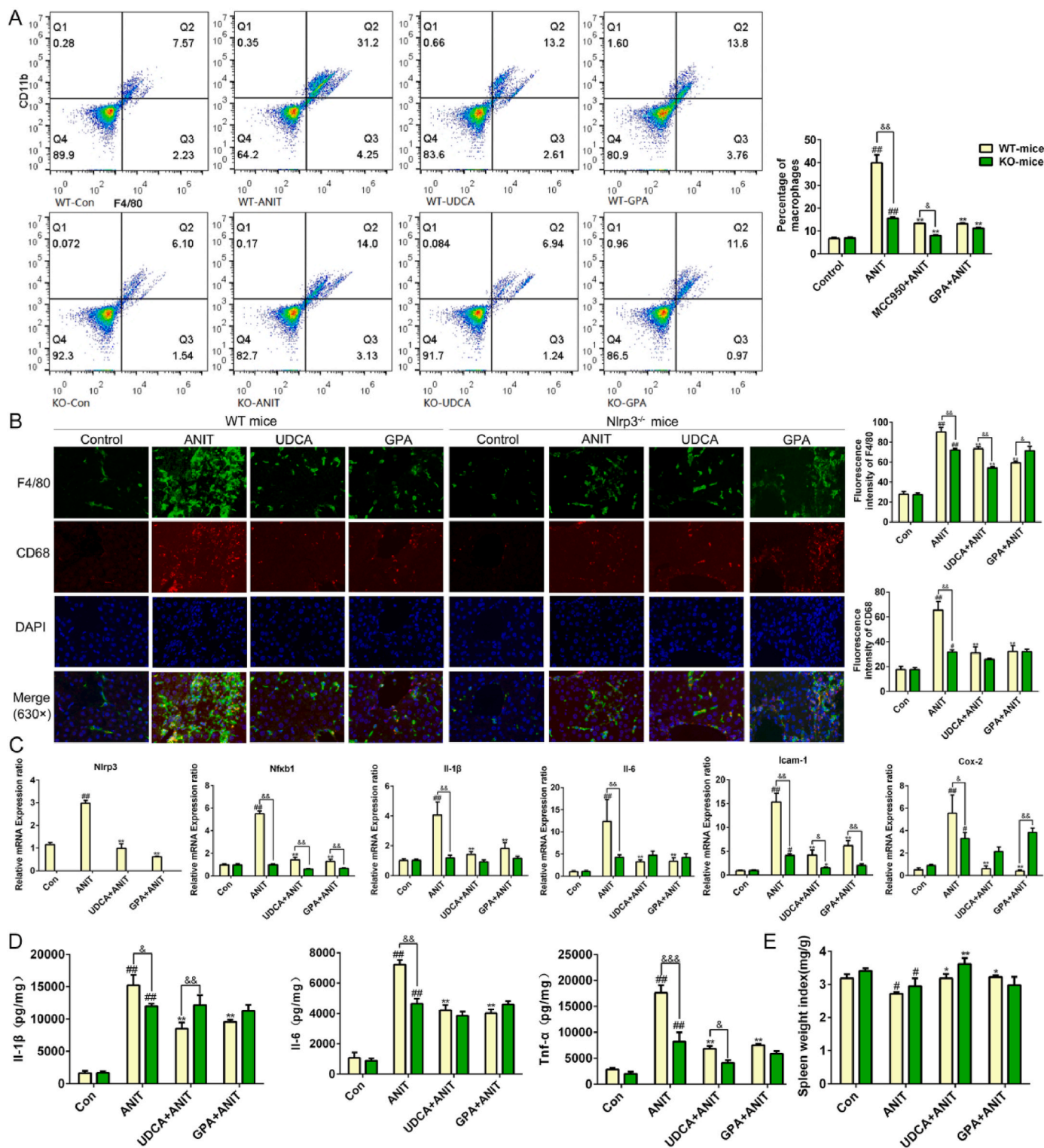
A clear hallmark of cholestasis is elevated BA levels in circulation and liver, which can trigger an inflammatory response by upregulating the expression of pro-inflammatory genes in hepatocytes and promoting

their release, including *IL-1 $\beta$* , *IL-6*, and *TNF- $\alpha$*  [38]. As a key inflammatory mediator in the upstream of the IL-6 and TNF- $\alpha$  signaling cascade, IL-1 $\beta$  is primarily generated via an NLRP3-dependent mechanism. Therefore, we investigated whether BAs could activate the NLRP3 inflammasome in hepatocytes as its activation in macrophages has been reported [10,22]. In cholestasis mouse, more than 99% of BAs in the liver and serum are conjugated, mainly comprising TCA and taur- $\alpha$ - $\beta$ -muricholic acid [39]. Animals exhibiting histopathological signs of bile duct hyperplasia also displayed elevated serum levels of TCA and glycocholate [40]. TCA-induced inflammation plays a more important role than the direct cytotoxic effects on hepatocytes, which contributes considerably to cholestatic liver fibrosis [39]. These results suggest that TCA play a critical role in cholestatic liver inflammatory injury. Thus, we clarified whether TCA-triggered inflammatory response is associated with the activation of NLRP3 inflammasome in hepatocytes. TCA significantly activated the NLRP3 inflammasome and stimulated the release of IL-1 $\beta$  and *Tnf- $\alpha$*  by upregulating *Nlrp3* and *Nfkb1* mRNAs in PMHs. This is consistent with a previous report that TCA remarkably enhanced *Il-1 $\beta$*  mRNA levels [3]. We hypothesized that high concentrations of unconjugated deoxycholic acid (DCA) and chenodeoxycholic acid (CDCA) could activate the NLRP3 inflammasome and stimulate the release of IL-1 $\beta$  in an NLRP3 inflammasome-dependent manner in macrophages, which is also supported by several studies [22]. However, Cai et al. reported that TCA had insignificant effects on NLRP3 inflammasome activation as indicated by the undetectable mRNA levels of *Il-1 $\beta$*  in PMHs and BMDMs [9]. In fact, TCA could induce the upregulation of *Nlrp3* mRNA in PMHs [9]; however, the reason for undetectable *Il-1 $\beta$*  mRNA levels remains unknown. Furthermore, Guo et al. reported that unconjugated BAs, including lithocholic acid (LCA) and CDCA, inhibit NLRP3 inflammasome activation [12]. Therefore, more studies exploring the role of the NLRP3 inflammasome in the pathogenesis of cholestatic liver injury should be conducted to address these controversial findings.

During cholestatic liver injury, BMDMs are recruited into the liver and then differentiate into self-renewing KCs, a subset of liver-resident macrophages derived from embryonic progenitors [41]. Activated KCs can secrete various mediators, including cytokines and chemokines, which would initiate liver immune response via communication with various liver cells, including hepatocytes and liver-resident KCs [38,42,43]. Indeed, the disruption of the communication between hepatic macrophages and hepatocytes via KC deletion protected against BDL- or LPS-induced acute cholestatic liver injury and inflammation [44–46], suggesting that the crosstalk between hepatic macrophages and hepatocytes plays a crucial role in the pathogenesis and resolution of cholestatic liver injury and inflammatory states [47]. However, whether the inflammatory response is directly triggered by the communication

between hepatic macrophages and hepatocytes remains to be elucidated. As BAs can directly initiate an inflammatory response by activating NLRP3 inflammasome signaling in hepatocytes, we speculate that the BA-initiated NLRP3 activation to release cytokines, such as IL-1 $\beta$  and TNF- $\alpha$ , may result in the recruitment of BMDMs into the liver to further activate NLRP3 signaling, thereby amplifying the hepatic inflammatory response and resulting in hepatocyte pyroptosis and the deterioration of liver inflammation. To verify this hypothesis, we first performed

conditional culture of PMHs and BMDMs and found that TCA could trigger liver inflammation by activating NLRP3 signaling via the communication between hepatic macrophages and hepatocytes. In addition, *Nlrp3* deficiency and its inhibition via MCC950 and GPA in both PHMs and BMDMs attenuated the inflammatory response induced by TCA. Mice with deleted *Nlrp3* or consumption of KCs were protected against ANIT-induced cholestatic liver inflammatory injury, whereas those with liver *Nlrp3*<sup>oe</sup> had exacerbated ANIT-induced cholestatic liver



(caption on next page)

**Fig. 7. Anti-inflammatory effect of GPA against ANIT-induced acute liver injury is largely abolished in *Nlrp3*-knockout mice.** WT mice and *Nlrp3*<sup>-/-</sup> mice were orally administered with the vehicle (0.5% carboxymethylcellulose), UDCA (75 mg/kg) as positive control, or GPA-H (100 mg/kg) once daily for seven days and with ANIT (100 mg/kg) on day 5. (A) Representative FACS image of mouse liver sample. After sacrificing the animals, liver macrophage were isolated, and the inflammatory infiltration was evaluated by FACS (n = 5). Data are expressed as the mean ± SEM of 5 independent mice liver samples (n = 5). \*P < 0.05, \*\*P < 0.01 versus vehicle-treated control group in WT and *Nlrp3*<sup>-/-</sup> mice; \*P < 0.05, \*\*P < 0.01 compared to ANIT-treated alone group. (B) Hepatic F4/80 and CD68 protein expression measured by immunofluorescence assay. The nuclei were stained with DAPI in blue, and targeted protein was stained in red (F4/80) or green (CD68) (magnification: 630 × ). Data are expressed as the mean ± SEM of 3 independent mice liver samples (n = 3). #P < 0.05, ##P < 0.01 versus vehicle-treated control group in WT and *Nlrp3*<sup>-/-</sup> mice; \*P < 0.05, \*\*P < 0.01 compared to ANIT-treated alone group. (C) Levels of NLRP3 and proinflammatory mRNAs in mouse liver were determined by real-time PCR. Data are expressed as the mean ± SEM of 5 independent mouse samples (n = 5). Results are expressed as fold changes compared to the vehicle-treated control group. #P < 0.05, ##P < 0.01 versus vehicle-treated control group in WT and *Nlrp3*<sup>-/-</sup> mice; \*P < 0.05, \*\*P < 0.01 compared to ANIT-treated alone group. (D) Levels of inflammatory cytokines including IL-1β, IL-6, and TNF-α in mouse liver were detected by ELISA. Data are expressed as the mean ± SEM of 5 independent mouse samples (n = 5). #P < 0.05, ##P < 0.01 versus vehicle-treated control group, \*P < 0.05, \*\*P < 0.01 versus ANIT-treated group. (E) Effects of GPA treatment on spleen weight index (ratio of spleen weight to body weight) of ANIT-induced mice. Data are expressed as the mean ± SEM of 5 independent mouse samples (n = 5). Results are expressed as fold changes compared to the vehicle-treated control group. #P < 0.05, ##P < 0.01 versus vehicle-treated control group in WT and *Nlrp3*<sup>-/-</sup> mice; \*P < 0.05, \*\*P < 0.01 compared to ANIT-treated alone group. (For interpretation of the references to colour in this figure legend, the reader is referred to the Web version of this article.)

injury. Consistent with our results, Isaacs-Ten et al. reported that BA-induced cell death is reduced in hepatocytes derived from germ-free mice, which lacked activation of the NLRP3 signaling, and that macrophage exhaust and inflammasome inhibition via MCC950 could alleviate ANIT-induced cholestatic liver injury [48]. Consistently, our results showed that GPA could suppress NLRP3 activation and protect against ANIT-induced cholestatic inflammatory injury in WT mice, but not in *Nlrp3*-deficient or macrophage-exhausted mice.

In summary, our findings demonstrate that TCA can promote the activation of NLRP3 inflammasome to induce pro-inflammatory cytokines release and subsequently trigger inflammatory responses in hepatocytes and macrophages. Hepatocyte-released pro-inflammatory cytokines contribute to the recruitment of macrophages into the liver that further activates the NLRP3 inflammasome of hepatic macrophages, thereby aggravating hepatocyte inflammation (Graphical abstract). The disruption of the mutual communication between hepatocytes and macrophages via the inhibition of NLRP3 activation or consumption of macrophages could mitigate ANIT-induced cholestatic liver inflammatory injury. In addition, we identified GPA could act as a specific NLRP3 inhibitor by covalently binding to NLRP3. GPA subsequently attenuated ANIT-induced cholestatic liver inflammatory injury in an NLRP3-dependent manner by blockage of the crosstalk between hepatocytes and macrophages. Overall, our findings serve as basis for further studies on the regulation of mutual communication between hepatocytes and hepatic macrophages as a potential therapeutic target for cholestasis.

## 4. Materials and methods

### 4.1. Animal experiments

Wild-type (WT) mice (C57BL/6 background) were obtained from Guangdong Medical Laboratory Animal Center (Guangzhou, China), and *NLRP3*<sup>-/-</sup> mice (C57BL/6 background) were purchased from The Jackson Laboratory (Bar Harbor, ME, USA). Both types of mice were housed in a barrier facility with a 12/12 h light/dark cycle, had free access to water and a normal chow diet.

To investigate the effect of GPA, mice were orally administered with 0.5% carboxymethylcellulose (as control group), UDCA (75 mg/kg; as positive control), or various concentrations of GPA (100, 50, and 25 mg/kg for high (GPA-H), medium (GPA-M), and low (GPA-L) groups, respectively) or intraperitoneally injected with MCC950 (20 mg/kg; positive control) once a day for seven days. At the day 5 or day 6, mice were intragastrically administered with ANIT (100 mg/kg, dissolved in soybean oil) or intraperitoneally injected with LPS (50 mg/kg) to induce cholestatic liver injury, respectively.

Mice with systemic macrophage consumption were generated by intraperitoneal injections of clodronate-loaded liposomes (herein, clodronate liposomes; 0.1 mL per 10 g mouse body weight) three days before the administration of MCC950 or GPA with PBS-loaded liposomes

(control group; herein, PBS liposomes; 0.1 mL per 10 g mouse body weight). During the administration period, mice were intraperitoneally injected with PBS or clodronate liposomes every two days to stabilize macrophage exhaust.

Mice with liver-specific *Nlrp3* overexpression were established using p-Adv-EF1-mScarlet-CMV-Nlrp3-3 × FLAG (herein, Adv-NLRP3). WT mice were intravenously injected with Adv-NLRP3 or pAdeno-EF1A(S)-mScarlet-CMV-MC5-3 FLAG (herein, Adv-con) three days before administration of MCC950 or GPA. Overexpression efficiency was examined using Western blot analysis.

After the above-mentioned pretreatment, mice were euthanized, serum were stored at -20 °C for further analyses, and livers were harvested and stored at -80 °C for biochemical and molecular biology analyses, or fixed in 4% formalin for histological assessment and immunofluorescence detection. All animal care and experimental protocols were approved by and in accordance with the guidelines of the Animal Ethics Committee of Guangzhou University of Chinese Medicine (approval No. 20201013002).

### 4.2. Chemicals and reagents

Primary antibodies against NLRP3 (ab214185), NF-κB (ab16502), IκBα (ab133462), and GAPDH (ab181602) were purchased from Abcam (Cambridge, UK); P-IκBα (2859s), P-NF-κB (3039s), and IL-1β (12242s) were purchased from Cell Signaling Technology (Denver, MA, USA); ASC (sc-271054), CASP-1(sc-56036), F4/80 (sc-377009), and β-ACTIN (sc-8432) were purchased from Santa Cruz Biotechnology (CA, USA). The pCDNA3.1 control plasmid, pGL3-CMV Renilla luciferase plasmid and pGL4.32-NF-κB-luc plasmid were purchased from Promega Co, LTD (Madison, Wisconsin, USA). The pCDNA3.1-hNLRP3 plasmid was the gift from Professor Wu Baojian (Jinan University).

GPA (C<sub>16</sub>H<sub>22</sub>O<sub>10</sub>; molecular weight [Mw] = 374.34) was acquired from Shanghai Acme Biochemical Co., Ltd (Shanghai, China); ursodeoxycholic acid (UDCA, C<sub>24</sub>H<sub>40</sub>O<sub>4</sub>; Mw = 392.57, U110695) and 1-Naphthyl isothiocyanate (ANIT, C<sub>10</sub>H<sub>7</sub>NCS; Mw = 185.24, N106389) were purchased from Shanghai Aladdin Biochemical Technology Co., Ltd. (Shanghai, China); MCC950 sodium (MCC950, Mw = 426.46, HY-12815A) and recombinant mouse macrophage colony stimulating factor (M-CSF, HY-P7085) were purchased from MedChemExpress (New Jersey, USA).

TaqMan probes, including those for human-specific *NLRP3* (Hs00918082), *NFκB1* (Hs00765730), *IL-1β* (Hs00174097), *IL-6* (Hs00174131), *ICAM-1* (Hs00164932), *COX-2* (Hs00153133), *TNF-α* (Hs00174128), and *GAPDH* (Hs02786624); and mouse-specific *Nlrp3* (Mm00840904), *Nfκb1* (Mm00476361), *Il-1β* (Mm00434228), *Il-6* (Mm00446190), *Icam-1* (Mm00516023), *Cox-2* (Mm00478374), *Tnf-α* (Mm00443258), *Cyp7a1* (Mm00484150), *Cyp8b1* (Mm00501637), *Cyp27a1* (Mm00470430), *Cyp2b10* (Mm01972453), *Cyp3a11* (Mm00731567), *Ugt1a1* (Mm02603337), *Abcb11* (Mm00445168),

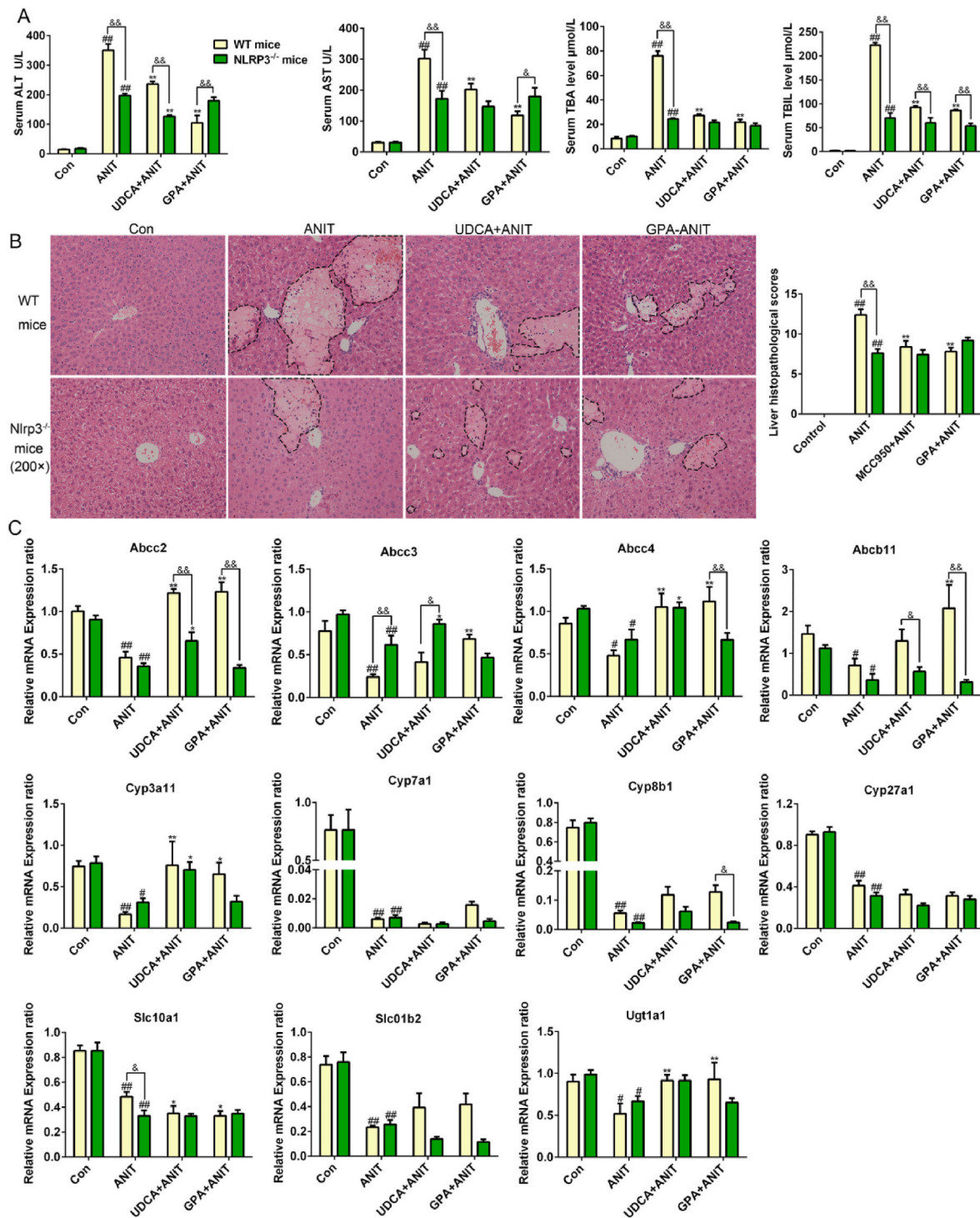


**Fig. 8. Hepatoprotective effect of GPA against ANIT-induced acute liver injury is partly mitigated in *Nlrp3*-knockout mice.** (A) Serum biochemical indexes of cholestatic liver injury including ALT, AST, TBA and TBIL levels were evaluated. Data are expressed as the mean ± SEM from 5 to 6 independent mice samples (n = 5–6). <sup>#</sup>*P* < 0.05, <sup>##</sup>*P* < 0.01 versus vehicle-treated control group in WT and *Nlrp3*<sup>-/-</sup> mice; \**P* < 0.05, \*\**P* < 0.01 compared to ANIT-treated alone group. (B) Representative images of haematoxylin and eosin staining in liver sections (magnification:200 × ). The circle indicated bleeding, inflammatory infiltration and hepatic necrosis. Data are expressed as the mean ± SEM of 5 independent mouse samples (n = 5). Results are expressed as fold changes compared to the vehicle-treated control group. <sup>#</sup>*P* < 0.05, <sup>##</sup>*P* < 0.01 versus vehicle-treated control group in WT and *Nlrp3*<sup>-/-</sup> mice; \**P* < 0.05, \*\**P* < 0.01 compared to ANIT-treated alone group. (C) Relative mRNA levels of BA synthesis- and transport-related genes in mouse liver were tested by real-time PCR. Data are expressed as the mean ± SEM of 5 independent mouse samples (n = 5). Results are expressed as fold changes compared to the vehicle-treated control group. <sup>#</sup>*P* < 0.05, <sup>##</sup>*P* < 0.01 versus vehicle-treated control group in WT and *Nlrp3*<sup>-/-</sup> mice; \**P* < 0.05, \*\**P* < 0.01 compared to ANIT-treated alone group.

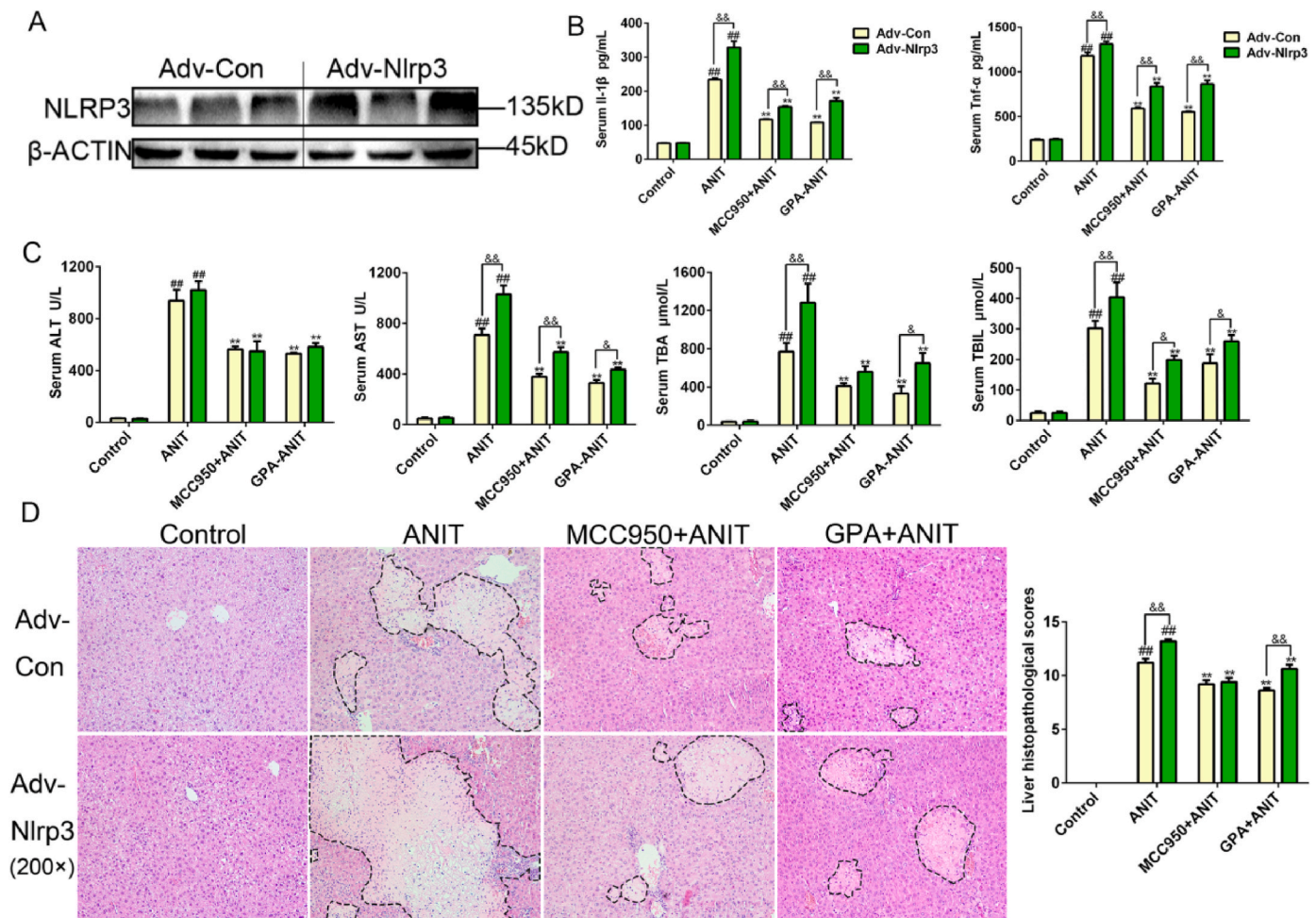


**Fig. 9.** Liver-specific overexpression of NLRP3 antagonizes the hepatoprotective effect of GPA against ANIT-induced acute inflammatory liver injury. WT mice were intravenously injected with Adv-Con or Adv-Nlrp3 adenovirus ( $1 \times 10^9$  pf) via the tail vein for three days and then orally administered with MCC950 (20 mg/kg) or GPA (100 mg/kg). On day 8, they were orally administered with ANIT (100 mg/kg) to induce acute liver injury. (A) Protein levels of NLRP3 in the liver tissues. Actin was used as internal reference protein. Data are expressed as the mean  $\pm$  SEM of 3 independent mouse samples ( $n = 3$ ). (B) Serum IL-1 $\beta$  and TNF- $\alpha$  levels were detected by ELISA. Data are expressed as the mean  $\pm$  SEM of 5 independent mouse samples ( $n = 5$ ).  $^{\#}P < 0.05$ ,  $^{\#\#}P < 0.01$  versus vehicle-treated control group in WT and *Nlrp3*<sup>oe</sup> mice;  $^*P < 0.05$ ,  $^{**}P < 0.01$  compared to ANIT-treated alone group. (C) Serum biochemical indexes of cholestatic liver injury including ALT, AST, TBA and TBIL levels were evaluated. Data are expressed as the mean  $\pm$  SE from 5 to 6 independent mice samples ( $n = 5-6$ ).  $^{\#}P < 0.05$ ,  $^{\#\#}P < 0.01$  versus vehicle-treated control group in WT and *Nlrp3*<sup>oe</sup> mice;  $^*P < 0.05$ ,  $^{**}P < 0.01$  compared to ANIT-treated alone group. (D) Representative images of haematoxylin and eosin staining in liver sections (magnification: 200 $\times$ ). The circle indicated bleeding, inflammatory infiltration and hepatic necrosis. Data are expressed as the mean  $\pm$  SE from 5 independent mice samples ( $n = 5$ ).  $^{\#}P < 0.05$ ,  $^{\#\#}P < 0.01$  versus vehicle-treated control group in WT and *Nlrp3*<sup>oe</sup> mice;  $^*P < 0.05$ ,  $^{**}P < 0.01$  compared to ANIT-treated alone group.

*Abcc2* (Mm00496899), *Abcc3* (Mm00551550), *Abcc4* (Mm01226381), *Slc01b2* (Mm00451510), *Slc10a1* (Mm00441421), and *Gapdh* (Mm99999915), were acquired from Invitrogen (Carlsbad, CA, USA). All other commercially available chemicals were of highest quality.

#### 4.3. Real-time quantitative PCR

Total RNA was extracted from mouse tissues or cells using TRIzol reagent (Sigma, St. Louis, MO, United States). Subsequently, the concentrations and purity of total RNA were measured using the NanoDrop 2000 Spectrophotometer (Thermo Fisher Scientific, Waltham, MA, USA), and then reverse-transcribed into cDNA using the High-capacity cDNA reverse transcription kits (Thermo Fisher Scientific, Waltham, MA, USA). A total 20  $\mu$ L cDNA (2000 ng) was amplified with TaqMan<sup>TM</sup> Fast Advanced Master Mix (Applied Biosystems, Carlsbad, CA, USA) on StepOnePlus system (Applied Biosystems) and 7500 Real-Time PCR System (Applied Biosystems). The GAPDH/*Gapdh* was used as the endogenous reference control, and the relative quantification for indicated genes expression was calculated using the comparative Ct method

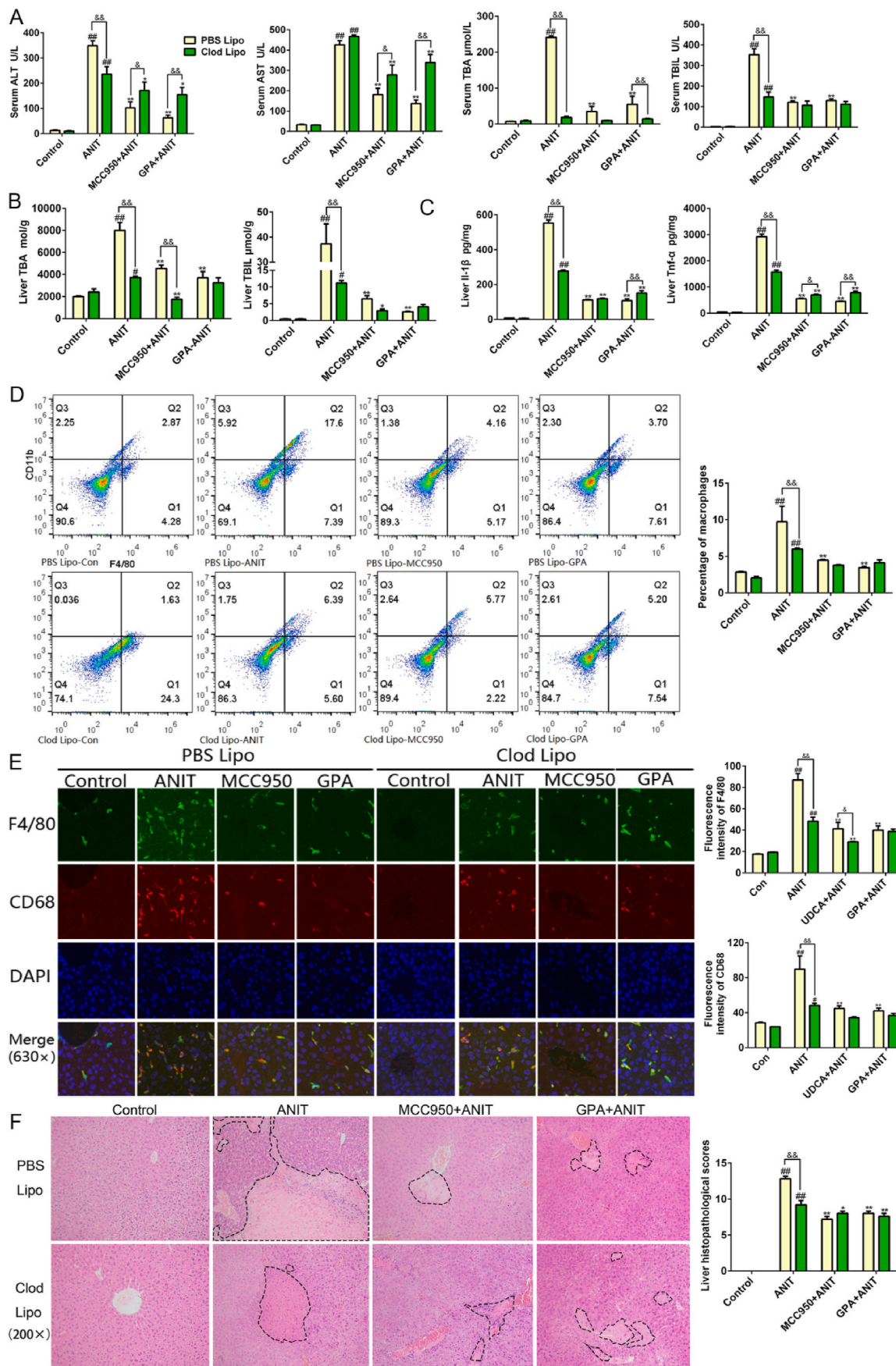
relative to the control/vehicle group.

#### 4.4. Cell culture and pretreatment

THP-1 monocytes were purchased from the American Type Culture Collection (Manassas, VA, USA), and MPHs were isolated from WT and *Nlrp3*<sup>-/-</sup> mice [49]. BMDM were obtained by perfusion with a 2-mL syringe, after which the cells were cultured and fully differentiated in medium containing M-CSF for 5–7 days. The cells were cultured in RPMI1640 medium with 10% fetal bovine serum (FBS), 100 U/mL penicillin, and 0.1 mg/mL streptomycin at 37  $^{\circ}$ C in a humidified 5% CO<sub>2</sub> incubator. All culture reagents were obtained from Gibco (Carlsbad, CA, USA).

#### 4.5. Western blot analysis

Proteins were extracted from liver tissues or cultured cells using RIPA buffer (Beyotime Institute of Biotechnology, Hangzhou, China) containing a cocktail of protease inhibitors and quantified using the BCA



(caption on next page)

**Fig. 10. GPA protection against ANIT-induced acute liver injury partially depends on macrophages activation.** WT mice were intraperitoneally injected with PBS Lipo (PBS liposomes) or Clod Lipo (Clodronate liposomes) for consecutive three days before the oral administration with MCC950 (20 mg/kg) or GPA (100 mg/kg). On day 8, they were orally administered with ANIT(100 mg/kg) to induce acute liver injury. **(A and B)** Serum (A) and liver (B) levels of ALT, AST, TBA, and TBIL of mice with ANIT-induced acute liver injury. Data are expressed as the mean  $\pm$  SEM of 6 independent mouse samples ( $n = 6$ ).  $^{\#}P < 0.05$ ,  $^{\#\#}P < 0.01$  versus vehicle-treated control group in PBS Lipo and Clod Lipo-treated mice;  $^*P < 0.05$ ,  $^{**}P < 0.01$  compared to ANIT-treated alone group. **(C)** Hepatic IL-1 $\beta$  and Tnf- $\alpha$  levels were detected by ELISA. Data are expressed as the mean  $\pm$  SEM of 6 independent mouse samples ( $n = 6$ ).  $^{\#}P < 0.05$ ,  $^{\#\#}P < 0.01$  versus vehicle-treated control group in PBS Lipo and Clod Lipo-treated mice;  $^*P < 0.05$ ,  $^{**}P < 0.01$  compared to ANIT-treated alone group. **(D)** Representative FACS image of mouse liver sample. After sacrificing the animals, liver macrophage were isolated, and the inflammatory infiltration was evaluated by FACS. Data are expressed as the mean  $\pm$  SEM of 5 independent mice liver samples ( $n = 5$ ).  $^{\#}P < 0.05$ ,  $^{\#\#}P < 0.01$  versus vehicle-treated control group in PBS Lipo and Clod Lipo-treated mice;  $^*P < 0.05$ ,  $^{**}P < 0.01$  compared to ANIT-treated alone group. **(E)** Hepatic F4/80 and CD68 protein expression measured by immunofluorescence assay. The nuclei were stained with DAPI in blue, and targeted protein was stained in green (F4/80) or red (CD68) (magnification: 630  $\times$ ). Data are expressed as the mean  $\pm$  SEM of 3 independent mice liver samples ( $n = 3$ ).  $^{\#}P < 0.05$ ,  $^{\#\#}P < 0.01$  versus vehicle-treated control group in PBS Lipo and Clod Lipo-treated mice;  $^*P < 0.05$ ,  $^{**}P < 0.01$  compared to ANIT-treated alone group. **(F)** Representative images of haematoxylin and eosin staining in liver sections (magnification:200  $\times$ ). The circle indicated bleeding, inflammatory infiltration and hepatic necrosis. Data are expressed as the mean  $\pm$  SEM of 5 independent mice liver samples ( $n = 5$ ).  $^{\#}P < 0.05$ ,  $^{\#\#}P < 0.01$  versus vehicle-treated control group in PBS Lipo and Clod Lipo-treated mice;  $^*P < 0.05$ ,  $^{**}P < 0.01$  compared to ANIT-treated alone group. (For interpretation of the references to colour in this figure legend, the reader is referred to the Web version of this article.)

assay (Guangzhou Dingguo Biology, Guangzhou, China). Equal concentrations of the samples were mixed with LDS sample buffer, separated using 8–15% SDS-PAGE gels, and transferred onto PVDF membranes, which were blocked with 5% non-fat milk in tris-buffered saline containing 0.1% Tween 20 (TBS-T) for 1.5 h at room temperature. Then, membranes were incubated with primary antibodies overnight at 4  $^{\circ}$ C, followed by incubation with HRP-conjugated secondary antibodies for 2 h at room temperature. After washing with TBS-T 3 times, ECL kits (Millipore Corporation, Billerica, USA) were used to detect the proteins. Protein bands were quantified using Image Lab and ImageJ software, and the relative amount of proteins were normalized to  $\beta$ -ACTIN or GAPDH.

#### 4.6. ELISA assay

Inflammatory cytokines in the serum samples, tissue supernatants, and cell-culture media were measured for mouse IL-1 $\beta$ , IL-6, or Tnf- $\alpha$  and human IL-1 $\beta$ , IL-6, or TNF- $\alpha$  using ELISA kits (ExCell Bio, Shanghai, China).

#### 4.7. Determination of intracellular ion levels

Potassium and calcium ion concentrations in cell lysates were detected using reagent kits from Jiancheng Bioengineering Institute (Nanjing, China).

#### 4.8. Analysis of biochemical indicators

Alanine aminotransferase (ALT), aspartate transaminase (AST), total BA (TBA), and total bilirubin (TBIL) in serum samples or liver homogenates were assayed using reagent kits from Jiancheng Bioengineering Institute (Nanjing, China).

#### 4.9. Preparation of bio-GPA

D-biotin was condensed with short-chain amino PEG to form a biotin-PEG molecule with an amino-protecting group. The amino-protecting group of the intermediate was removed using a dichloromethane solution containing 30% trifluoroacetic acid to obtain the modified amino-PEG-biotin.

Then, GPA was dissolved in pyridine solution and added with 20  $\times$  excess acetic anhydride to acetylate all hydroxyl groups. The obtained acetylated GPA was amidated with modified amino-PEG-biotin to generate acetylated Bio-GPA that was dissolved in 20 mM sodium methoxide solution and stirred at room temperature for approximately 30 min to remove the acetyl group, thereby producing the final product, bio-GPA.

Bio-GPA: 1H NMR (400 MHz, MeOD)  $\delta$  7.24 (d,  $J = 0.9$  Hz, 1H), 5.78 (s, 1H), 5.15 (d,  $J = 7.4$  Hz, 1H), 4.70 (d,  $J = 7.9$  Hz, 1H), 4.50 (dd,  $J =$

7.8, 4.5 Hz, 1H), 4.35–4.28 (m, 2H), 4.19 (d,  $J = 14.5$  Hz, 1H), 3.86 (d,  $J = 11.8$  Hz, 1H), 3.69–3.59 (m, 10H), 3.59–3.32 (m, 12H), 3.28 (dd,  $J = 8.5, 6.5$  Hz, 3H), 3.26–3.19 (m, 2H), 2.93 (dd,  $J = 12.8, 5.0$  Hz, 1H), 2.83–2.68 (m, 3H), 2.22 (t,  $J = 7.3$  Hz, 2H), 2.07 (dd,  $J = 16.1, 7.7$  Hz, 1H), 1.80–1.54 (m, 5H), 1.49–1.40 (m, 2H).

#### 4.10. Pull-down assay

THP-1 monocytes were stimulated with 1  $\mu$ g/mL LPS for 24 h. Lysates were collected and centrifuged at 6500  $\times$  rpm, and the supernatants were collected and incubated with 20  $\mu$ L streptavidin magnetic beads (New England Biolabs, USA) for 4 h at 4  $^{\circ}$ C to integrate unspecified binding proteins. After mixing, the sample pellets were discarded by centrifugation. The supernatants were collected and incubated with bio-GPA or GPA for 6 h at 4  $^{\circ}$ C, and streptavidin magnetic beads were added to the supernatants overnight at 4  $^{\circ}$ C. After centrifugation, the supernatants were collected as “after pull-down”, and then the lysates were added to mix the precipitates, followed by boiling and centrifuging to collect the supernatants as “pull-down”.

Purified recombinant human NACHT, LRR, and PYD domains-containing proteins (NLRP3, CUSABIO, Wuhan, China) were dissolved in lysis buffer, and then incubated with bio-GPA, GPA or/and  $\beta$ -Me for 6 h at 4  $^{\circ}$ C, followed by incubation with streptavidin beads overnight at 4  $^{\circ}$ C.

#### 4.11. Haematoxylin and eosin staining of liver tissues

Liver tissues were washed with normal saline, dehydrated, embedded in paraffin, fixed in 10% buffered formalin, sectioned (5  $\mu$ m thick), deparaffinized, and stained with haematoxylin and eosin (H&E) for histological evaluation. Slides were visualized under a light microscope (Olympus, Tokyo, Japan).

#### 4.12. Immunofluorescence analysis

BMDM and differentiated THP-1 monocytes ( $2\text{--}3 \times 10^5$ /mL) were seeded in a 24-well plate, pretreated with DMSO or indicated concentrations of GPA for 24 h, treated with LPS for 24 h (1.0  $\mu$ g/mL), or followed by induction of ATP (2.5 mM) for 30 min. After washing for three times with PBS, the cells were fixed with paraformaldehyde for 20 min. Cells were washed three times with PBS, permeabilized using 1% Triton X-100 in PBS for 15 min, and then blocked with 5% BSA for 1 h at room temperature. The blocking solution was aspirated, and a sufficient amount of diluted primary antibodies was added to cover the cells, after incubating with the primary antibodies for NF- $\kappa$ B (dilution 1:200, Abcam), NLRP3 (1:200, Abcam), and ASC (1:200, Santa Cruz) overnight at 4  $^{\circ}$ C. This was followed by incubation with secondary antibodies (Invitrogen) for 60 min at room temperature. The cells were then counter-stained with DAPI in PBS for 20 min at room temperature. After

washing in PBS for 3 times, cells images were visualized under a fluorescence microscope (Olympus).

Liver sections were deparaffinized, rehydrated with graded series of ethanol, and incubated with 3% H<sub>2</sub>O<sub>2</sub> in distilled water for 10 min to complete hot antigen retrieval. The liver sections were blocked with 5% BSA for 1 h at room temperature before incubating with the primary antibodies for F4/80 (1:200, Santa Cruz), and CD68 (1:200, Santa Cruz) overnight at 4 °C followed by incubation with secondary antibodies (Invitrogen) for 60 min at room temperature. Subsequently, the slides were counterstained with DAPI in PBS for 20 min at room temperature. After washing in PBS for 3 times, liver images were visualized under a fluorescence microscope (Olympus).

#### 4.13. Hepatic BAs determination

The quantification of individual BA levels in liver tissue was carried out our previously published method with minor modifications [50]. Namely, pulverized liver tissues was homogenized using 5 fold volume of methanol/water (6:4, v/v) containing an internal standard. After centrifugation, the protein levels of mixtures were quantitated using the BCA assay (Guangzhou Dingguo Biology, Guangzhou, China). Then, the supernatants were dried with nitrogen at 45 °C, and residues were reconstituted with 100 µl methanol and 5 µl of the supernatants were injected to the ultra-performance chromatography-electrospray tandem mass spectrometry (UPLC-MS/MS) for analysis. The individual BA levels were normalized according to the BA levels divided by the corresponding protein concentrations.

#### 4.14. Determination of intracellular and hepatic ROS levels

The intracellular ROS levels in BMDM and THP-1 monocyte cells were measured as our previously reported methods [51]. After pretreatment with indicated concentrations of GPA for 24 h, cells (2–3 × 10<sup>5</sup>/mL) were continued to treated with LPS (1.0 µg/mL) for another 24 h, followed by addition of ATP (2.5 mM) for 30 min. Then, cells were incubated with ROS fluorescent probe DHE (5 µM, KeyGEN BioTECH, Cat#:KGAF019) at 37 °C for 0.5 h in a 5% CO<sub>2</sub> humidified incubator. Cells were washed with PBS and observed under a fluorescence microscope (Olympus).

For measurement of mouse hepatic ROS generation, mice were intragastrically pretreated with GPA (100, 50, and 25 mg/kg) and UDCA (75 mg/kg) for 5 day. At the day 5, mice were intragastrically administered with ANIT (100 mg/kg), and followed by GPA and UDCA treatment for another 2 days. In the day 7, mice were injected with DCFH-DA (10 mM, 10 µl) via tail vein 1 h before killing, and their livers were harvested. Hepatic ROS levels were determined using Berthold Technologies LB983 NC100 as our previous methods [51].

#### 4.15. Dual-luciferase reporter assay

HEK293T or RAW264.7 cells (1 × 10<sup>5</sup>/mL) in 96-well plates were transiently transfected with pCDNA3.1, pCDNA3.1-hNLRP3 (100 ng per well), or pGL4.32-NF-κB (200 ng per well) and pGL3-CMV Renilla luciferase plasmid (10 ng per well) (Transheep, Shanghai, China) as an internal control using Lipofectamine 2000TM (Invitrogen, Carlsbad, CA, USA). After transfection for 12 h, cells were treated with DMSO (vehicle control), GPA-H (100 µM), GPA-M (50 µM), GPA-L (25 µM), and MCC950 (10 µM) for 12 h before with or without 24 h-induction of LPS (1.0 µg/mL).

After incubation, the dual luciferase reporter detection system (Promega, Madison, Wisconsin, USA) was used to measure firefly and Renilla activities on the Enspire multi-mode plate reader (PerkinElmer, CA, USA). The firefly luciferase activity was normalized to that of Renilla luciferase.

#### 4.16. Flow cytometry assay

After perfusion and tear, MPHs were isolated and removed, and the supernatants were centrifuged at 1500 rpm for 3min. The resultant supernatants were further collected (supernatant 1). While the resultant precipitation were resuspended with PBS and further centrifuged twice at 50 g for 3min to obtain the supernatants (supernatant 2). Then, the supernatant 1 and supernatant 2 were combined and mixed, and centrifuged again at 500 g for 5min. The resultant precipitation was collected and resuspended with PBS, which was gently added to 3 ml separation solution containing 33% Percoll. After centrifuge at 1500 g for 20 min, crude macrophages from mouse liver tissue were extracted for subsequent Flow cytometry assay.

Cells (6 × 10<sup>5</sup>) were resuspended with 100 µl PBS, followed by addition with F4/80 fluorescent antibody and CD11b fluorescent antibody (Invitrogen, CA, USA). The mixture was incubated at room temperature for 25 min away from light. After incubation, 1.5 mL PBS was added into the mixture and centrifuged at 1000 g for 5 min at room temperature. After washing for removal of the residual antibody, the resultant precipitation was resuspended and then detected by BD flow cytometry.

#### 4.17. Statistical analyses

All values in the figures are expressed as the mean ± SEM. Data analysis was performed in GraphPad Prism Version 6.0 (GraphPad Software, La Jolla, CA, USA) using one-way ANOVA followed by LSD or Dunnett's. *P*-values < 0.05 were considered statistically significant.

#### Author contributions

M. Song and C. Liu conceived the study; the majority of experiments were designed and performed by M. Song, T. Zhi, S Lin, N. Luo, Y. Gao, and C. Liu, assisted by Z. Chen, R. Qiu, F Chen, F. Liu, C. Shen and F. Zhang; T. Zhi, Z. Chen, W. Xie, Y. Zhou and R. Qiu contributed greatly to the animal experiments and performed oral gavage, intraperitoneal injection and intravenous injection procedures; M. Song and S. Lin analyzed the data; C. Liu and M. Song wrote the manuscript with input from the other authors.

#### Disclosures

The authors declare no competing financial interests.

#### Declaration of competing interest

The authors declare no conflicts of interests.

#### Acknowledgments

This work was supported by the Natural Science Foundation of China (82174032, 81773969, 81800738 and 82070891), and Science and Technology Key Program of Guangzhou (202002020032), and “double first-class” and high-level university discipline collaborative innovation team project of Guangzhou University of Chinese Medicine (2021xk79).

#### Appendix A. Supplementary data

Supplementary data to this article can be found online at <https://doi.org/10.1016/j.redox.2022.102404>.

#### References

- [1] N.S. Ghonem, D.N. Assis, J.L. Boyer, Fibrates and cholestasis, *Hepatology* 62 (2) (2015) 635–643.
- [2] P. Fickert, et al., Characterization of animal models for primary sclerosing cholangitis (PSC), *J. Hepatol.* 60 (6) (2014) 1290–1303.

- [3] K. Allen, H. Jaeschke, B.L. Copple, Bile acids induce inflammatory genes in hepatocytes: a novel mechanism of inflammation during obstructive cholestasis, *Am. J. Pathol.* 178 (1) (2011) 175–186.
- [4] S.Y. Cai, et al., Bile acids initiate cholestatic liver injury by triggering a hepatocyte-specific inflammatory response, *JCI Insight* 2 (5) (2017), e90780.
- [5] M.S. Dick, et al., Corrigendum: ASC filament formation serves as a signal amplification mechanism for inflammasomes, *Nat. Commun.* 8 (2017), 15030.
- [6] C.J. Gross, et al., K(+) efflux-independent NLRP3 inflammasome activation by small molecules targeting mitochondria, *Immunity* 45 (4) (2016) 761–773.
- [7] S. Paik, et al., An update on the regulatory mechanisms of NLRP3 inflammasome activation, *Cell. Mol. Immunol.* 18 (5) (2021) 1141–1160.
- [8] M. Frissen, et al., Bidirectional role of NLRP3 during acute and chronic cholestatic liver injury, *Hepatology* 73 (5) (2021) 1836–1854.
- [9] S.Y. Cai, et al., Inflammasome is activated in the liver of cholestatic patients and aggravates hepatic injury in bile duct-ligated mouse, *Cell Mol Gastroenterol Hepatol* 9 (4) (2020) 679–688.
- [10] L. Yang, et al., Regulation of epithelial injury and bile duct obstruction by NLRP3, IL-1R1 in experimental biliary atresia, *J. Hepatol.* 69 (5) (2018) 1136–1144.
- [11] J. Qu, et al., The selective NLRP3 inflammasome inhibitor MCC950 alleviates cholestatic liver injury and fibrosis in mice, *Int. Immunopharm.* 70 (2019) 147–155.
- [12] C. Guo, et al., Bile acids control inflammation and metabolic disorder through inhibition of NLRP3 inflammasome, *Immunity* 45 (4) (2016) 944.
- [13] H. He, et al., Oridonin is a covalent NLRP3 inhibitor with strong anti-inflammasome activity, *Nat. Commun.* 9 (1) (2018) 2550.
- [14] S. Wang, et al., REV-ERB $\alpha$  integrates colon clock with experimental colitis through regulation of NF- $\kappa$ B/NLRP3 axis, *Nat. Commun.* 9 (1) (2018) 4246.
- [15] M. Sendler, et al., NLRP3 inflammasome regulates development of systemic inflammatory response and compensatory anti-inflammatory response syndromes in mice with acute pancreatitis, *Gastroenterology* 158 (1) (2020) 253–269, e14.
- [16] J. Tang, et al., Sequential ubiquitination of NLRP3 by RNF125 and Cbl-b limits inflammasome activation and endotoxemia, *J. Exp. Med.* 217 (4) (2020).
- [17] G. Ren, et al., ABRO1 promotes NLRP3 inflammasome activation through regulation of NLRP3 deubiquitination, *EMBO J.* 38 (6) (2019).
- [18] R. Malireddi, et al., TAK1 restricts spontaneous NLRP3 activation and cell death to control myeloid proliferation, *J. Exp. Med.* 215 (4) (2018) 1023–1034.
- [19] R. Zhou, et al., A role for mitochondria in NLRP3 inflammasome activation, *Nature* 469 (7329) (2011) 221–225.
- [20] M.W. Azeltine, et al., Inflammation drives MicroRNAs to limit hepatocyte bile acid transport in murine biliary atresia, *J. Surg. Res.* 256 (2020) 663–672.
- [21] H. Chen, et al., Geniposidic acid protected against ANIT-induced hepatotoxicity and acute intrahepatic cholestasis, due to Fxr-mediated regulation of Bsep and Mrp2, *J. Ethnopharmacol.* 179 (2016) 197–207.
- [22] H. Hao, et al., Farnesoid X receptor regulation of the NLRP3 inflammasome underlies cholestasis-associated sepsis, *Cell Metabol.* 25 (4) (2017) 856–867, e5.
- [23] I. Giovannini, et al., Sepsis-induced cholestasis, *Hepatology* 47 (1) (2008) 361.
- [24] L. Hao, et al., ERR $\gamma$  suppression by Sirt6 alleviates cholestatic liver injury and fibrosis, *JCI Insight* 5 (17) (2020).
- [25] Y.H. Youm, et al., The ketone metabolite beta-hydroxybutyrate blocks NLRP3 inflammasome-mediated inflammatory disease, *Nat. Med.* 21 (3) (2015) 263–269.
- [26] M. Cocco, et al., Development of an acrylate derivative targeting the NLRP3 inflammasome for the treatment of inflammatory bowel disease, *J. Med. Chem.* 60 (9) (2017) 3656–3671.
- [27] K. Sato, et al., Pathogenesis of kupffer cells in cholestatic liver injury, *Am. J. Pathol.* 186 (9) (2016) 2238–2247.
- [28] F. Tacke, Targeting hepatic macrophages to treat liver diseases, *J. Hepatol.* 66 (6) (2017) 1300–1312.
- [29] A.J. Greaney, et al., Sulforaphane inhibits multiple inflammasomes through an Nrf2-independent mechanism, *J. Leukoc. Biol.* 99 (1) (2016) 189–199.
- [30] M.J. Daniels, et al., Fenamate NSAIDs inhibit the NLRP3 inflammasome and protect against Alzheimer's disease in rodent models, *Nat. Commun.* 7 (2016), 12504.
- [31] C. Marchetti, et al., OLT1177, a beta-sulfonyl nitrile compound, safe in humans, inhibits the NLRP3 inflammasome and reverses the metabolic cost of inflammation, *Proc. Natl. Acad. Sci. U. S. A.* 115 (7) (2018) E1530–E1539.
- [32] Y. He, et al., 3,4-methylenedioxy-beta-nitrostyrene inhibits NLRP3 inflammasome activation by blocking assembly of the inflammasome, *J. Biol. Chem.* 289 (2) (2014) 1142–1150.
- [33] Y. Shi, et al., Ginsenoside Rg3 suppresses the NLRP3 inflammasome activation through inhibition of its assembly, *Faseb. J.* 34 (1) (2020) 208–221.
- [34] A. Hooftman, et al., The immunomodulatory metabolite itaconate modifies NLRP3 and inhibits inflammasome activation, *Cell Metabol.* 32 (3) (2020) 468–478, e7.
- [35] V. Petrilli, et al., Activation of the NALP3 inflammasome is triggered by low intracellular potassium concentration, *Cell Death Differ.* 14 (9) (2007) 1583–1589.
- [36] Y. He, et al., NEK7 is an essential mediator of NLRP3 activation downstream of potassium efflux, *Nature* 530 (7590) (2016) 354–357.
- [37] G.S. Lee, et al., The calcium-sensing receptor regulates the NLRP3 inflammasome through Ca<sup>2+</sup> and cAMP, *Nature* 492 (7427) (2012) 123–127.
- [38] C.L. Scott, et al., Bone marrow-derived monocytes give rise to self-renewing and fully differentiated Kupffer cells, *Nat. Commun.* 7 (2016), 10321.
- [39] Y. Zhang, et al., Effect of bile duct ligation on bile acid composition in mouse serum and liver, *Liver Int.* 32 (1) (2012) 58–69.
- [40] J. Tian, et al., Galectin-3 regulates inflammasome activation in cholestatic liver injury, *Faseb. J.* 30 (12) (2016) 4202–4213.
- [41] S. Yona, et al., Fate mapping reveals origins and dynamics of monocytes and tissue macrophages under homeostasis, *Immunity* 38 (1) (2013) 79–91.
- [42] V.K. Verma, et al., Alcohol stimulates macrophage activation through caspase-dependent hepatocyte derived release of CD40L containing extracellular vesicles, *J. Hepatol.* 64 (3) (2016) 651–660.
- [43] C.L. Elsegood, et al., Kupffer cell-monocyte communication is essential for initiating murine liver progenitor cell-mediated liver regeneration, *Hepatology* 62 (4) (2015) 1272–1284.
- [44] C. Jones, et al., Hepatic cytokine response can be modulated using the Kupffer cell blocker gadolinium chloride in obstructive jaundice, *Int. J. Surg.* 11 (1) (2013) 46–51.
- [45] S. Abraham, et al., Kupffer cell blockade improves the endotoxin-induced microcirculatory inflammatory response in obstructive jaundice, *Shock* 30 (1) (2008) 69–74.
- [46] E. Sturm, et al., Kupffer cell depletion with liposomal clodronate prevents suppression of Ntcp expression in endotoxin-treated rats, *J. Hepatol.* 42 (1) (2005) 102–109.
- [47] Z. Shan, C. Ju, Hepatic macrophages in liver injury, *Front. Immunol.* 11 (2020) 322.
- [48] A. Isaacs-Ten, et al., Intestinal microbiome-macrophage crosstalk contributes to cholestatic liver disease by promoting intestinal permeability in mice, *Hepatology* 72 (6) (2020) 2090–2108.
- [49] F. Cabral, et al., Purification of hepatocytes and sinusoidal endothelial cells from mouse liver perfusion, *JoVE* (132) (2018).
- [50] R. Zhang, et al., Xiaoyan lidan formula ameliorates alpha-naphthylisothiocyanate-induced intrahepatic cholestatic liver injury in rats as revealed by non-targeted and targeted metabolomics, *J. Pharm. Biomed. Anal.* 179 (2020), 112966.
- [51] N. Sun, et al., Hepatic Kruppel-like factor 16 (KLF16) targets PPAR $\alpha$  to improve steatohepatitis and insulin resistance, *Gut* 70 (11) (2021) 2183–2195.